SEPTEMBER 2018

M.Sc. in Electrical and Electronics Engineering

ISRAA HASAN RIFAHT

UNIVERSITY OF GAZİANTEP

GRADUATE SCHOOL OF

NATURAL & APPLIED SCIENCES

RELIABILITY ANALYSIS OF CONCRETE FILLED STEEL TUBE MEMBERS OF QUADRILATERAL AND CIRCULAR CROSS SECTIONS

M. Sc. THESIS

IN

CIVIL ENGINEERING

BY

ISRAA HASAN RIFAHT

SEPTEMBER 2018

Reliability Analysis Of Concrete Filled Steel Tube Members Of Quadrilateral And Circular Cross Sections

M.Sc. Thesis

in

Civil Engineering

University of Gaziantep

Supervisor

Assist. Prof. Dr. Mehmet Tolga GÖĞÜŞ

by

Israa Hasan Rifaaht

September 2018

REPUBLIC OF TURKEY
UNIVERSITY OF GAZİANTEP
GRADUATE SCHOOL OF NATURAL & APPLIED SCIENCES
CIVIL ENGINEERING DEPARTMENT

Name of the thesis: Reliability Analysis of Concrete Filled Steel Tube Members of Quadrilateral and Circular Cross Sections.

Name of the student: Israa Hasan RIFAAHT

Exam date: 07.09.2018

Approval of the Graduate School of Natural and Applied Sciences

Prof. Dr. Ahmet Necmeddin YAZICI
Director

I certify that this thesis satisfies all the requirements as a thesis for the degree of Master of Science.

Prof. Dr. Hanifi ÇANAKÇI
Head of Department

This is to certify that we have read this thesis and that in our consensus opinion it is fully adequate, in scope and quality, as a thesis for the degree of Master of Science.

Asst. Prof. Dr. Mehmet Tolga GÖĞÜŞ
Supervisor

Examining Committee Members:	Signature
Assoc. Prof. Dr. Nildem TAYŞİ	....
Asst. Prof. Dr. Hasan Erhan YÜCEL	....
Asst. Prof. Dr. Mehmet Tolga GÖĞÜŞ	....

I hereby declare that all information in this document has been obtained and presented in accordance with academic rules and ethical conduct. I also declare that, as required by these rules and conduct, I have fully cited and referenced all material and results that are not original to this work.

Israa Hasan RIFAAHT

ABSTRACT

RELIABILITY ANALYSIS OF CONCRETE FILLED STEEL TUBE FOR QUADIRLATE AND CIRCULAR CROSS SECTIONS

RIFAAHT, Israa Hasan
M.Sc. in Civil Engineering
Assist. Prof. Dr. Mehmet Tolga GÖĞÜŞ
September 2018
68 pages

Concrete filled steel tube beams is a structural composition that brings the advantages of the combination of the surrounding steel with the core concrete, this structural member had been investigated under different conditions but still, there is a significant difference among the well-known design codes provisions and limitations. Assessing the limit states of the codes can be conducted based on structural reliability analysis. Bending capacity of the beams can be characterized by the reliability index in terms that can be readily understood by structural engineers with only a basic knowledge of probability theory. In this study, First-order Reliability Method was used in assessing the selected tested specimens. More than 2000 concrete filled steel tube members of different shapes cross-section had been collected from recently introduced literature (from 2000 up to 2018); moreover, the selected specimens were compared with the provisions of many codes. The judgment was based on the convergences between the calculated beams load capacity in term of bending strength according to mentioned codes and the recorded load and moment capacity that obtained from the experimental work. Different parameters were evaluated from the selected beams, columns and beam-column. The material properties are also altered in order to evaluate its effect on the members strength, where the concrete compressive strength was ranging between 10 to 154 MPa, and the steel yield strength was less than 762 MPa. The results show that both codes (EC4-2004 and AISC360-10) have percentages of error within the unsafe zone, and EC4 is less conservative than the AISC.

Keywords: CFST beams, Bending strength, Design codes, Structural safety, Reliability

ÖZET

DÖŞEME VE DOLAŞIMLI KESİTLER İÇİN BETON DOLDURULMUŞ ÇELİK TÜPÜNÜN GÜVENİLİRLİK ANALİZİ

RIFAAHT, Israa Hasan
Yüksek Lisans Tezi, İnşaat Mühendisliği
Danışman: Yard. Doç. Dr. Mehmet Tolga GÖĞÜŞ
Eylül 2018
68 Sayfa

Beton doldurulmuş çelik tüp kirişleri, çevredeki çeliğin çekirdek betonla kombinasyonunun avantajlarını getiren yapısal bir bileşimdir, bu yapısal eleman farklı koşullar altında araştırılmıştır, ancak yine de, tanınmış tasarım kodları kuralları ve sınırlamaları arasında önemli bir farklar vardır. Tasarım kodların limit durumlarının değerlendirilmesi, yapısal güvenilirlik analizine dayalı olarak gerçekleştirilebilir. Kirişlerin eğilme kapasitesi, yapı mühendisleri tarafından sadece temel bir olasılık teorisi bilgisi ile kolayca anlaşılabilen, güvenilirlik indeksi ile karakterize edilebilir. Bu çalışmada, seçilen test edilen numunelerin değerlendirilmesinde birinci dereceden güvenilirlik yöntemi kullanılmıştır. Farklı kesit şekillerindeki 2000'den fazla Beton doldurulmuş çelik tüp elemanları, yakın zamanda sunulan literatürden (2000'den 2018'e kadar) toplanmıştır; ayrıca, seçilen örnekler birçok kodun kurallarına göre karşılaştırılmıştır. Sonuçlar, belirtilen kodlara göre eğilme mukavemeti açısından hesaplanan kiriş yük kapasitesi ile deneysel çalışmadan elde edilen sunulan yük kapasitesi arasındaki yakınsamaya dayanmaktadır. Seçilen kirişlerde farklı parametreler değerlendirilirken, ana parametreler olarak kirişlerin geometrisi, tüp kalınlığı, elemanların genişliği arasında değişmektedir. Beton dayanım mukavemeti 10 ila 154 MPa arasında değişen kiriş mukavemeti üzerindeki etkisini değerlendirmek için malzeme özellikleri de değiştirilmiş ve çelik akma dayanımı 762 MPa'dan az olmuştur. Sonuçlar, her iki kodun da (EC4-2004 ve AISC360-10) güvensiz bölgede hata yüzdesine sahip olduğunu ve EC4'ün de AISC'den daha az konzervatif olduğunu göstermektedir.

Anahtar Kelimeler: Beton doldurulmuş çelik tüp kirişleri, Eğilme dayanımı, Tasarım kodları, Yapısal güvenlik, Güvenilirlik

To my parents, My sistermy, niece Meryam

ACKNOWLEDGEMENT

At first, thank God for everything I have reached, and then I would like to express my sincere gratitude to my supervisor **Assist. Prof. Dr. Mehmet Tolga GÖĞÜŞ** for the continuous support of my M.Sc study and research, for his patience, motivation, enthusiasm, and immense knowledge. His guidance helped me in all the time of research and writing of this thesis. I'm very grateful and proudest to work under his academic guidance.

Special thanks to my **family**. Words cannot express how my grateful to my **father** to encourage me and my **mother** for support me all my life, and my **sister** which was always by my side, for their strong encouragement during the years of my study.

CONTENTS

Page

LIST OF FIGURES

Page

LIST OF TABLE

Page

ABBREVIATIONS

CCFST	Circular Concrete Filled Steel Tube
RCFST	Rectangular Concrete Filled Steel Tube
AISC360-10	American Institute of Steel Construction 2010
EC4-2004	Euro Code 2004
PSDM	Plastic Stress Distribution Method
SCM	Strain Matching Method
HSS	Hollow Steel Section
GLM	General Linear Model
BS	British Standard
AIJ	Architectural Institute of Japan
AS	Australian Standard
LRFD	Load Resistance Factor Design
ASD	Allowable Stress Design
FORM	First Order Reliability Method
MVFOSM	Mean Value Of First Order Second Moment Method

LIST OF SYMBOLS

Symbols according to AISC360-10

Specified compressive strength of concrete $(MPa) f_c'$

Specified minimum yield stress of the steel $(MPa) F_y$

Modulus of elasticity of concrete = $(0.043 wc\ 1.5\sqrt{f\ c'},) E_c$

Modulus of elasticity of steel = $(200000\ MPa) E_s$

Weight of concrete per unit volume $(1500 \leq wc \leq 2500\ kg\ m3 /) w_c$

B Width of rectangular HSS member (mm)

H Height of rectangular HSS member (mm)

t Wall thickness of HSS member (mm)

Base of an HSS rectangular concrete cross-section $(bc = b - 2t) b_c$

h_c Depth of rectangular concrete cross-section $(h\ c = h - 2t)$

r Radius of gyration of the cross-section

Cross-sectional area of steel section $(mm2) A_a$

Area of concrete $(mm2) A_c$

Steel cross-section moment of inertia $(mm4) I_s$

Concrete cross-section moment of inertia $(mm4) I_c$

Plastic section modulus of steel $(mm3) Z_s$

Plastic section modulus of concrete $(mm3) Z_c$

Nominal compressive strength $(N) P_n$

Nominal compressive strength of zero length $(N) P_{no}$

Euler or elastic critical buckling load $(N) P_e$

Nominal bearing strength $(N)P_p$

Axial yield strength $(N)P_y$

Effective stiffness of composite section $(N - mm2)EI_{eff}$

Critical stress $(MPa)F_{cr}$

k Effective length factor

L laterally unbraced length of the member (mm)

λ Slenderness parameter

Limiting slenderness parameter for compact elementλ_p

Limiting slenderness parameter for non-compact elementλ_r

Nominal flexural strength $(N - mm)\mathrm{M}_n$

Plastic bending moment $(N - mm)\mathrm{M}_p$

Moment at yielding of the extreme fiber $(N - mm)\mathrm{M}_r$

Symbols according to EC4-2004

Design value of cylinder compressive strength of concrete (MPa) f_{cd}

f_{ck} Characteristic value of the cylinder compressive strength of concrete 28 days (MPa)

Design value of the yield strength of structural steel $(MPa)f_{yd}$

Nominal value of the yield strength of structural steel $(MPa)f_y$

Modulus of elasticity of structural steel =210000 $N\ mm2/EcmE_a$

Secant modulus of elasticity of concrete (MPa)

Cross-sectional area of the structural steel section $(mm2)A_a$

Cross-sectional area of concrete $(mm2)A_c$

Second moment of area of the structural steel section $(mm4)I_a$

Second moment of area of the un-cracked concrete section $(mm4)I_c$

Design value of the plastic resistance moment of the composite$M_{pl,Rd}$

section $(N - mm)$

Design value of the plastic resistance of the composite section to$N_{pl,Rd}$

compressive normal force (N)

Characteristic value of the plastic resistance of the composite $N_{pl,Rk}$
section to compressive normal force (N)

Elastic critical normal force $(N) N_{cr}$

χ Reduction factor for flexural buckling

δ Factor; steel contribution ratio; central deflection

λ Relative slenderness

Reliability analysis symbol

Reliability indexβ

S Load or moment taken from test result

R Load or moment taken from codes

Mean for load or moment taken from test resultμ_S

Mean for load or moment taken from codesμ_c

Standard deviations for load or moment taken from test resultσ_R

Standard deviations for load or moment taken from codesσ_R

SF Safety factor

pf probability failure

ϕ The standard normal distribution can be taken from z-table

P_s Reliability percentage

C.O.V Coefficient of variation

CHAPTER 1

INTRODUCTION

1.1 General

Recently, CFST is increasingly being used other types of structures such as skyscrapers and bridge it has advantages compared with ordinary rebar or reinforced concrete columns. For the disadvantage of using a positive composite effect, two different materials compensated, combined benefits, efficient structure member. Because steel tube is a form for casting concrete, the necessary labor for shape and reinforcing rods are omitted. This leads to a cleaner of the building position and can be realized reductions in construction workers, project period and construction costs. Regarding structural performance, since this section provides the highest efficiency contribution to bending strength and cross-sectional moment of inertia of steel materials. Since steel tubes act both in the longitudinal and transverse directions, reinforced steel is not required for CFST. Includes lateral reinforcement for a concrete core. Concrete core is local buckle the steel tube by preventing inner buckling. Continuous confinement concrete is effectively strengthened by being supplied to the concrete core by the steel tube to improve strength and ductility, thus increasing CFST loading capacity. Therefore, with CFST, the available floor space is required column cross-sectional size. Increase in load capacity due to confinement of concrete depending on several parameters such as the strength and strength provided by the steel tube deformability of material, Length to diameter ratio (L/D) the ratio of diameter to thickness of steel tube (D/t), the eccentricity of load to diameter ratio(e/D), and sectional shape (for example, (Kenji Sakino *et al.*, 2004); (Walter Luiz Andrade Oliveira *et al.*, 2009); (Dundu, 2012); (Perea, 2010). In addition, concrete shrinkage and bonding between steel and concrete tubes play an important role in the axial load capacity of CFST members. The bond strength can be increased by adding Expanding Additive (EA) in concrete mix to reduce concrete shrinkage. This type of CFST member, Expansive Concrete Filled Steel Tube (ECFST).

The behavior of the CFST column using the traditional concrete mixture is significantly affected by the difference in poisson's ratio of steel and concrete. Since the Poisson's ratio of concrete is slightly lower than the Poisson's ratio of steel and the steel tube wall it is separated from the concrete core at the initial load stage. As it increases in the case of axial load, the lateral deformation of the concrete reaches that of steel tube, it develops tensile hoop stress as an example,(Sakino *et al.*, 2004).

Therefore, in the CFST column, the confinement effect of the steel tube in the concrete core, it receives a high level of axial load. On the other hand, in the ECFST column, expansion tendency of expanded concrete after casting, collide with the steel tube, and thus a preload containment effect is generated in front of the column and is loaded in the axial direction. Due to changes in the material properties of the concrete core in ECFST, the overall mechanical properties of the column inevitably change, it affects the supporting ability of the structural member. As a result of recent research, concrete is a promising technology to improve the performance of CFST columns by strengthening confinement and delaying the local buckling of steel tubes, this (For example, (Wang *et al.*, 2011); (Chang, Huang and Chen, 2009)). There it is an urgent need to bridge the gap of knowledge on the impact of concrete strength, concrete mixing approach, EA ratio, and cross sectional dimensions and slenderness especially the ratio of Expansive Concrete Filled Steel Tube ECFST to axial load capacity using Expansive Additive EA material it is commonly used in rural construction industry in United Arab Emirates UAE. (Lazkani, 2016)

More applications of CFST was founded such as in high rise building as shown in Figure 1.1.

There are five types of steel-concrete

(a) En Cased Steel (b) Normal CFST (c) Double skin section as shown

(d) Combination of CES (e) Hollow steel section as shown in Figure 1.2.

Figure 1.1 The application of CFST in high rise buildings

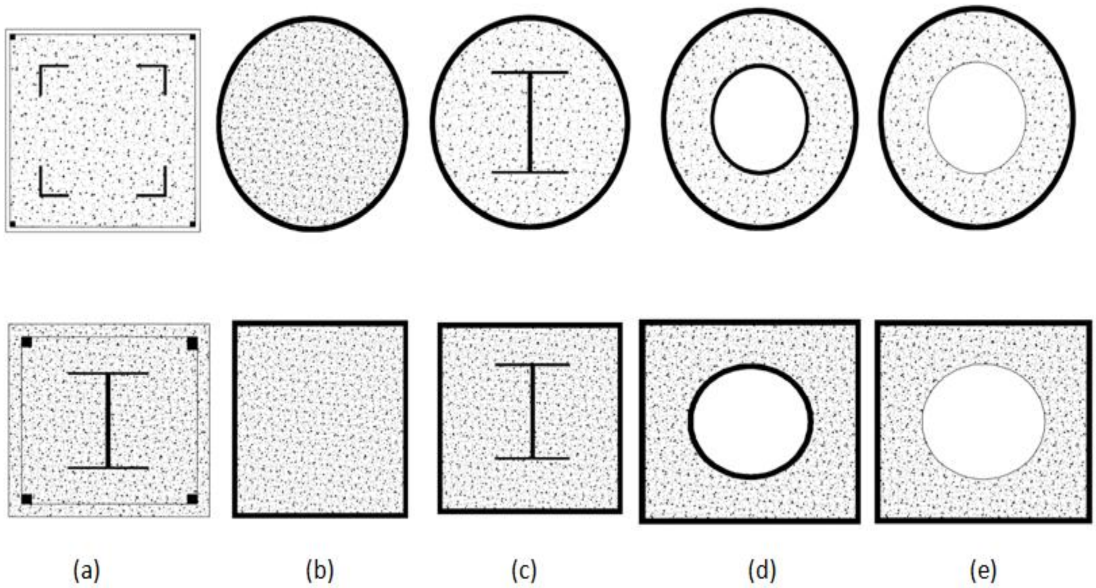

Figure 1.2 Types of concrete filled steel tube

With these types of CFSTs, the size of the column decreasing when compared with ordinary reinforced concrete column necessary to carry it. Therefore, considerable economic savings can be taken. Also, as for column size reduction, it is advantageous when floor space such as office space and the parking lot is important. Into, in addition, closely spaced composite columns connected to the spun-outside the high-rise building for lateral load resistance by the flat plate concept (Lazkani, 2016).

The steel composite section wrapped in concrete has many earthquake resistance construction. When the concrete column cracks under severe flight overload, the rigidity the steel core provides sheer ability and ductility resistance subsequent overload cycle. In addition, the surface area of the enclosed steel section, because the concrete cover was not damaged, there was no cost to paint and fire prevention. Concrete filling columns of steel tubes (CFST) have many earthquake resistant structures, high columns high strain rate bridge piers from troughs and railroad decks, concrete in order to use the filled steel tube, the structure is important. In the CFST structure, it can be used as a formwork and a ringing system for cast concrete under construction. Further, CFST provides high compression and torsional resistance for all axes. Steel composite section wrapped in concrete. (Abdalla, 2012).

1.2 Significance of Research

In the present time, the concrete-filled steel tube members are widely used in many construction works. In fact, these members are favored in practice because of its small cross-sectional area to load carrying capacity ratio. Therefore, the giant concrete columns in tall buildings' lower floors can be substituted by smaller sections of CFST columns.

So, CFST members can be used as piers for bridges at congested areas. Therefore, such structural members should be thoroughly investigated before used in critical structures. Despite being a research topic for around 50 years, the reliability analysis of the CFST members with codes is not studied. Thus, intensive parametric studies should be performed in order to find out which codes are best suited to measure loads and moments capacity and whichever more near for results experimental work. In this study, the reliability will be made between experimental work results and design codes results.

1.3 Objectives

1. The research aimed to collect experimental data from the literature in order to assess the following parameters:
   - The compressive strength of the concrete (fc') infill in order to make reliability between experimental result and codes for (fc') within code limit and (fc') out of limit code.

- The steel tube outer dimension to thickness ratio.
- Type of member (column, beam, or beam-column)
- shape of member

2. Moreover, the following standard code formulae are considered in the comparison:

   a. American Institute of Steel Construction code formulae (AISC).

   b. Euro Code 4 formula EC4-2004

1.4 Concrete Filled Steel Tube

1.4.1 Advantages of Concrete-Filled Steel Tubes:

The published concrete filling steel tube has many advantages, but it is an advantage that the system has in the construction order. The advantages of CFST columns are:

- Increased rigidity, leading to increased buckling resistance, and reduced the slenderness.
- Increase in strength for a given cross sectional dimension.
- By changing concrete strength, steel thickness, and reinforcement, similar cross sections with different moments and load resistances can be generated. This makes it possible to keep the outer dimensions of the column constant over the number of the eighth floor of the building, simplifying construction and structural details.
- Concrete strength increases due to the confinement effect of the steel tube, and deterioration of strength is not so severe in order to prevent repelling of concrete.
- Local buckling of steel tubes was delayed, and strength reduction after local buckling brought the restraining effect of concrete
- Creep of concrete and dry shrinkage is much smaller than an ordinary reinforced concrete column.
- Steel ratio (steel area / total area) of CFST cross section is much larger than steel ratio of the reinforced concrete section.

- In the structures subject to seismic reinforcement, the composite column can provide better ductility and load retention even after extensive concrete damage. If the entire structure survives, damage can be repaired
- CFST columns are very useful for rehabilitation of structures such as bridge piers and skyscrapers.
- Shape and reinforcement bars are unnecessary and concrete casting is done by the pump-up method, which saves manpower, structural cost and time.
- Because technology does not require a formwork, its location is clear and more space is available for male and machine movements. (Identity *et al.*, 2017).

1.4.2 Shapes of CFST members

There are many forms for the concrete filled steel tubes based on the confining steel tube's shape, such as square, rectangular, circular, elliptical, etc. As shown in Figure 1.3.

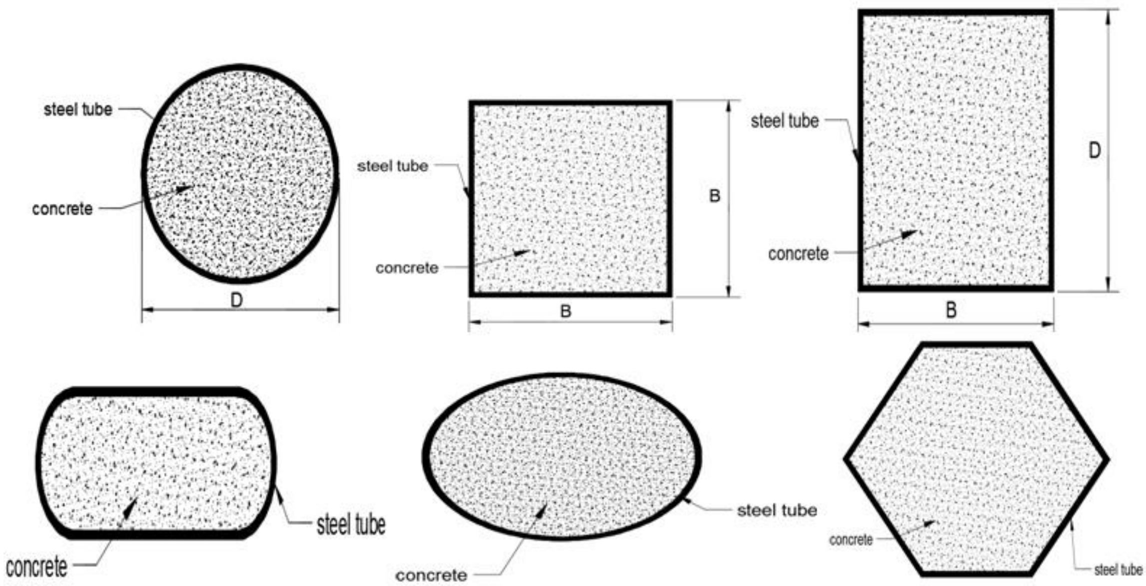

Figure 1.3 Shapes of CFST

Square and circular cross sections of CFST are widely used in construction. The loading and moment carrying capacity of the CFST column and the beam are greatly influenced by the ratio of the diameter to the thickness of the cross section width to thickness ratio of the steel tube. When static loading is applied, deformation of the circular CFST column experiences elastic complete plasticity or strain hardening behavior after shrinkage. On the other hand, the steel column for hollow structure showed a load deformation curve with the reduced yield at the same load.

1.5 Reliability Analyses:

1.5.1 Reliability Analyses

The reliability suggests that the scale produces a stable result if the estimate is modified in various situations. The inspect unreliable quality is called reliability investigation. A reliable quality inspection is determined by acquiring an accurate variety range at the scale that must be possible by determining the relationship between the scores obtained from the various organizations of the scale. Thus, if the relationship in the reliability survey is high, the scale gives predictable results and thus is safe.

1.5.2 The Aim of Reliability

1. Apply engineering relations and ideal methods to avoid stochastic probabilities of disasters or to reduce the probabilistic frequency of disasters.
2. Recognize and correct the reason for failure.
3. Adjust the way to suppress let-down. The cause is not adjusted.
4. Apply techniques to evaluate the possibility of new designs and analyze reliability information. (A, Khan and Kumar, 2017).

1.4.3 Structural Reliability Methods

As it is found in the literature, there are many methods are proposed to evaluate the reliability such as

1. First Order - Second Moment Concept (FOSM).

2. First Order Reliability Method (FORM).

3. Monte Carlo Simulation Method.

In this research, FORM was used to calculate the reliability percentage.

1.4.4 First Order Reliability Methods (FORM)

In the current research, FORM had been conducted the FORM-Concept (Hasofer and Lind 1974) is based on Description of reliability problem in standard Gaussian space. The conversion from the correlated non-Gaussian variable X to uncorrelated Gaussian variable U with zero mean and unit variance is therefore required. This step is called Rosenblatt transformation. Linearization is then performed in u space. The extension point u* is chosen to maximize the pdf in the failure region. Geometrically, this is consistent with a point in the faulty region with minimum distance β from the origin. From the viewpoint of safety engineering, design the point x* corresponding to u*. (Bucher and Bucher, 2011)

1.5 Lay Out

The research contains five chapters summarizing and dividing each chapter as follows:

Chapter 1. Introduction:

The objective and scope of the thesis were presented.

Chapter 2. Literature Review:

Previous studies were reviewed and maintained on the basis of the scope of the study. The CFST literature, general background, and parameters were reviewed which affect the performance of the CFST bending moment capacity and axial load.

Chapter 3. Methodology:

This Chapter, design of CFST structure by EC4-2004 Part2 and design of the composite concrete and steel structure in AISC360-10. Then from these design code, the comparison will be making by reliability analysis between resistance obtained from the design code and the actual test result. These methods are used in the calculation of Chapter 4 on the bending moment and axial load capacity for beam and column and beam-column.

Chapter 4. Results And Discussion:

Results will be provided for the distribution sheet used to calculate axial load, bending moment, and the results of the investigation as well as the results obtained using First Order Reliability Method (FORM) to determine the effect of the parameters.

Chapter 5. Conclusions:

Provide summaries and conclusions based on the results of comparative verifications of this study, and have recommended for future works.

CHAPTER 2

LITERATURE REVIEW

2.1 General

CFST are produced in different cross-section and, such as, rectangular CFST and Circular CFST, moreover different test configuration are found in the literature such as column CFST and beams CFST that were reinforced or non-reinforced.

The reliability of the nonlinear structure has received an increased interest in the past 20 years and important research has continuously contributed to this subject.

In this chapter, the previous studies are mentioned about

- The behavior of concrete filled steel tube.
- Reliability analysis of concrete-filled steel tube.

2.2 Behavior Of Concrete Filled Steel Tube

2.2.1 Beam

Lin Hai Han (2004) this study tested rectangular and square tubes infilled with normal concrete the main parameters diverse in the test were the depth to the width ratio between 1 to 2, and the tube depth to the wall thickness ratio are between 20 to 50. Comparisons are made with predicted moment capacity of the beam and flexural stiﬀ ness using the existing codes, such as EC4-1994, Architectural Institute of Japan, AIJ-1997, British Standard BS5400-1979, and American Institute of Steel Construction LRFD-AISC-1999. Generally, LRFD-AISC-1999 and AIJ-1997 gave a moment capacity 20% less than the actual test result, BS5400-1979 gave a moment capacity 12% less than the test result. EC4-1994 and the suggested method predicted about 10% lower capacity than the actual test results, are the best predictor. The method of AIJ-1997 can be used to calculate the bending stiffness of concrete-filled steel Squire Hollow Section SHS and Rectangular Hollow Section RHS beams because it predicts that the initial stiffness ki is slightly lower and the section stiffness ks value is slightly higher than the test results.

Arivalagan Soundararajan 2017 This paper presented 15 simple supported beam specimens of 1200 mm long steel hollow filled with fly ash, normal mix, low strength, and quarry waste concrete, with the same dimensions of the hollow It experimented. The extensive measurements of such material properties, deflection and strain were made. For comparison, this study also calculated theoretical studies of the final flexural strength of the beam sample. These experimental findings showed that fly ash, normal mix, low strength, and quarry waste concrete improve the moment carrying capacity of steel hollow sections. The ultimate flexural strength of filled beams is increased by 16 % for low strength concrete and 25 % for normal mix concrete, fly ash concrete and quarry waste concrete. All specimens showed good post-yield behavior with good ductility performance.

Zhijian Yang 2017 studied eight specimens were prototyped to investigate the pure bending behavior test data of high strength concrete-filled steel beams using CFRP (carbon fiber reinforced polymer) were used to verify Finite Element Analysis (FEA) modeling and good agreement was generally achieved. Furthermore, the effect of yield strength, concrete strength, steel ratio and thickness of CFRP on the bending performance of the specimen was analyzed by FEA. According to the analysis of the bending moment versus the strain curve, the materials of the CFRP steel tube and concrete worked well under pure bending before the Carbon Fiber Reinforced Polymers CFRP tube ruptured. The results presented in this paper show that these composite beams have a very ductile response, as the composite is defined by CFRP tubes and steel tubes. The flexural response of the beam including flexural rigidity and final load can be greatly improved by the inner CFRP tube. Parametric research provides information on the development of equations to calculate moment capacity. Comparison between experimental failure load and predicted failure load shows good agreement. The bending response of the beam, including flexural rigidity and ultimate support capacity, can be greatly improved by internal CFRP tubing. And the internal CFRP tube improves the corner limit the effect of the square tube.

Hassanein (2017) tested six samples of Glass Fibre Reinforced Cementitious Material Filled Square Steel Tubular GFCMFST beams with lengths from 1100 mm to 1400 mm. For comparison, a rectangular steel tube beam filled with an unreinforced Cementitious Material Filled Steel Tubular CMFST is also prepared and tested. In the test, two shear spans versus depth ratios are taken into account. This test showed that all the beams had significant yielding plateau flat and therefore showed adequate ductility. In addition, it was found that the initial cracking of the filler occurred against the CMFST beam at lower loading levels compared to GFCMFST and had a higher compressive strength. It was also found that the stress of the CMFST beam is always greater than the corresponding value of the GFCMFST beam in both the compression zone and the tension zone. After that, the experimental moment capacity was compared with the available design method. It is recommended to use the estimated design strength after EC4-2004. Comparison of experimental results of initial and practical level flow stability with corresponding values from literature and design specifications was also made. Among the different methods, it was found that AIJ standard gives the most suitable results for the initial cross-sectional stability and the maintainability level section stability of the present composite beam. The result is that, firstly, increasing the compressive strength of the filling mixture from 55.4 to 62.1 MPa (10% increase) only increases the cross-sectional area capacity of the spar by 2%, using a mix with less fc' It is effective. Comparing the ductility, using glass fibers, even when the compressive strength of the matrix is lower than the base material of much higher compressive strength, the overall absorbed energy and ductility of the tested part are It was found to be improved.

Arivalagan (2010) This paper tested 15 samples under static load and nine samples under cyclic reversal load present studies on the bending and periodic behavior of hollow beam sections of concrete-filled steel. Test specimens filled with fly ash concrete, normal mixed concrete, quarry waste concrete, and low strength concrete (butt-brick - lime concrete) and hollow steel sections were tested. Distortion and deflection measurements were made under two-point loading. A theoretical model for predicting moment carrying capacity was also developed. The beam capacity was compared with the final volume obtained using international standards Euro Code 4 EC4-1994, ACI-2002 and American Institute of Steel Construction AISC-LRFD-1999. Experimental investigations have shown that the moment carrying capacity increases based on the compressive strength of the filler material. Because of the filling material the energy absorption capacity also increases. The analysis result shows good agreement with the experimental result. The test results show that the moment holding the capacity of quarry waste concrete, fly ash concrete and ordinarily mixed concrete increases by 25%, 27%, and 28%, respectively when compared with the hollow steel section. Concrete filling increases the residual load capacity of thin rectangular hollow section RHS and squares hollow section SHS beams to resist cyclic loads, especially when lateral displacement increases.

Cheng Fang (2018) In this article the behavior of stainless Square and Rectangular Hollow Sections SHS, and RHS under mutual constant uniaxial cyclic bending and constant compression Figure 1 show the details of specimens. A total of ten samples were tested, covers various section slenderness, bending direction, and axial load ratio. These test parameters were found to have a clear influence on the local buckling resistance of the specimen. It was also observed that the categorization limitations codified at the moment underestimate the ability of the stainless steel part to generate plastic elongation. The specimen showed low to moderate ductility and energy dissipation capability as local buckling occurs relatively early. The rationality of the current main design code for predicting the strength of the stainless steel member was also evaluated, and the design code turned out to have the following tendency. In consideration of ductility, the final drift is (0.3 to 11.2)%, the corresponding ductility coefficient is in the range of 1.00 to 4.68, decreasing as the wall thickness decreases, in the case of strong axial bending.

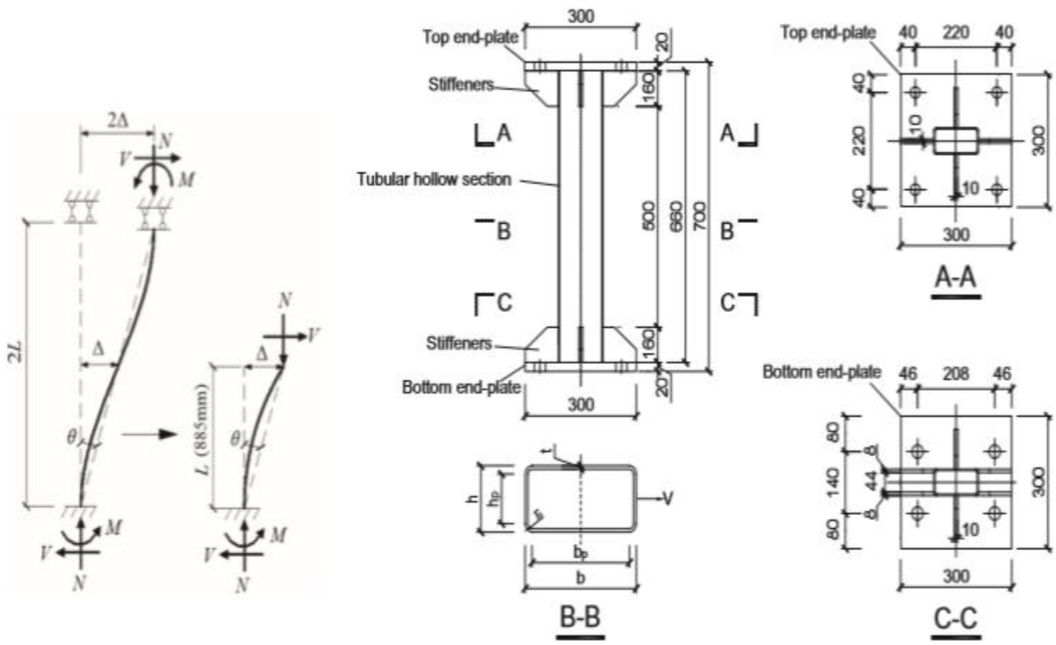

Figure 2.1 The details of the specimen

2.1.2 Column

Ahmed Elremaily (2002) the behavior of concrete filled column under static load was investigated by testing six columns subjected to the constant axial load in addition to periodic lateral load. The test parameters include the ratio of the steel tube diameter to the thickness, the compressive strength of the concrete, and the level of the axial load. The test column showed maintained its strength until the end of the test and high ductility. The test results also showed that due to the strength of the concrete obtained from the structure provided by the steel tube the column capacity was significantly improved. An analytical model was developed to predict the ability of Circular Concrete Filled Tube CCFT beam column considering the interaction between concrete and steel material. Comparing the experimental data reported in this paper with the data reported by other researchers, the Concrete Filled Tube CFT column shows a very high level of energy dissipation and ductility. The diameter-to-thickness ratio is 51, and a relatively high-level axial load, for example, 40% of the squash load, indicates that the displacement ductility ratio reaches a value of 10. Also, observed that the test piece maintains its capacity to the test results.

Hongcun Guo (2012) presented the experimental work on the tests of 9 concrete filled rectangular and square hollow section (HSS) columns Exposure to uniaxial bending or biaxial bending, axial load. Experimental results proposed that a total buckling appears with local buckling near the mid-height of the column. A good agreement was found between the experimental deflection shape and the semi-sine wave shape. It can be seen that the cross section remains flat before the sample reaches its load holding capacity. In addition, the experimental results are compared with the values calculated from the design codes of AISC-LRFD, EC4-2004, and it has been shown that all codes provide safe proof stress. Compared to pillars subjected to axial loading or uniaxial bending, the computational capacity of pillars subjected to biaxial deflection is more conservative. Among these three design codes, the capacity based on EC4-2004 design code has the closest result to the experiment result. The result calculated from the AISC-LRFD design code is the most conservative. The results show that the design based on AISC-LRFD code was more conservative and it conservatively estimates the load capacity by more than 60%.

An experimental study has been done by Soner Guler (2013) about square high strength Steel Fiber Reinforced Concrete SFRC fill of steel tube column subjected to axial load. A series of experiments were conducted to investigate the behavior of the high strength SFRC filled steel tube column and the effect of the D/t ratio on the axial load capacity and the joint strength of concrete and steel tube. In order to investigate the adhesion effect on the axial load capacity, the sample is separated into a grease state and a non-grease state. A total of 13 specimens are tested and compared with AISC, ACI, EC4-2004, and Australian Standard (AS) code. From this result, it was confirmed that the difference in the axial load capacity of the non-grease-like high strength SFRC packed tube column is important. All design codes overestimate the axial load capacity of specimens with thinner steel tube thickness (D/t ratio 33.3). Bond stress capacity is much higher than columns with thinner steel tube walls (smaller D/t ratio) columns. The differences in the axial load capacity of grease and nongreasy test specimens of 5 mm, 4 mm, 3 mm steel pipe thickness are 10%, 13%, and 14%, respectively.

Faisal Hafiz (2016) presents numerical and analytical studies on the behavior of CFST columns was applied to the axial compressive load. For this purpose, the axial strength of the CFST column and the corresponding confinement factor were evaluated using the Chinese code CESC 28: 90 design mechanism and Eurocode-4 EC4 design mechanism. Numerical analysis is performed using 3-dimensional nonlinear finite element software ABAQUS 6.13. The proposed finite element model is verified by comparing the result with the results of the corresponding experimental specimen. The obtained analysis result and numerical result are compared. For this study, twelve circular CFST specimens with different thicknesses and steel tubs filled with different grade of concrete are selected from the literature. The results show that the CFST column under the axial compressive load is not affected by the change in effective length.CFST columns with a small ratio of diameter to thickness indicate a sharp decrease in concrete confinement.

Fa xing Ding (2018) in this paper, theoretical and experimental studies of Carbon Fiber Reinforced Polymer CFRP Confined Concrete Filled Circular Steel Tube (CCFT) stub columns are carried out and the purpose is to examine the strength of concrete on the difference of the number of CFRP layers and the mechanical performance of CFRP restricted CFT stub columns. it was based on continuum dynamics which is a machine model of a concentric cylinder consisting of a cylinder, concrete core, CFRP, was founded and a corresponding elastic plastic method obtained by the FORTRAN program. The effect of the ductility, constraining effect of the steel tube on the core concrete and the number of CFRP layers on the ultimate capacity was considered and identified. Finally, based on the critical equilibrium and elasto-plastic method, a simplified formula for the final capacity of CFRP composed CFT stub columns was suggested. The experimental results showed that the greatest inconsistency between the elastoplastic method and the proposed formula was less than 12%, and a good agreement of the final capacity was found. Based on the elasto-plastic method, A theoretical model was established for considers the axial load of CFT's concentric cylinder by CFRP. The influence of structural CFRP between concrete and steel tube was identified. In the CFT stub column defined by CFRP, the radial and axial stresses of the concrete were greatly improved before the CFRP was crushed. At the same time, the axial stress of steel tube decreased due to tensile stress. In addition, the effect of the steel tube on concrete decreased slightly as the number of CFRP layers increased. Therefore, it can be concluded that the adhesion from the steel tube to the concrete core is somewhat weakened by the constraint of CFRP.

Yiyan Lu (2014) In this article, the results of experimental studies on the behavior of concrete-filled steel tubular columns surrounded by Fiber Reinforced Polymer FRP are introduced. 11 columns were tested to verify the influence of FRP layer number, steel tube thickness and strength of concrete on yield strength and the axial deformation capacity. Experimental results showed that FRP wrap effectively restricts the expansion of concrete and retards local buckling of steel tube. The axial deformability and loading capacity of steel tubular columns filled with concrete can be substantially improved by FRP confinement. A model has been Suggested to predict the load capacity of a concrete-filled steel tube column confined by FRP. The expected results are generally in good agreement with the experimental results obtained in this research and the literature.FRP wrap delays twisting local buckling deformation of the steel tube and the lateral expansion of the concrete of the CFST column can be suppressed. The strength and strain capacity of concrete can be reinforced by additional confinement from FRP wrap. Glass Fiber Reinforced Polymer GFRP wrap has higher strain competence than Carbon Fiber Reinforced Polymer CFRP wrap. CFRP efficiency decreases with increasing concrete strength but increases with increasing number of CFRP layers.

2.1.3 Beam-Column

YEH (2004) tested 19 CFT square samples with a common width (B) of 280 mm and width to thickness (B/t) ratio of 70 and. The specified (B/t) ratio does not meet the requirements for most design codes. 15 samples of these test samples were tested under bending loads and the remaining samples were tested under repeated bending loads. The corresponding simulation was also performed by the fiber division method due to the impact of steel and concrete bonding. It was observed that the reinforced CFT beam columns had better curvature performance with respect to weld capacity and the curvature of bending than non-reinforced. The improvements are more pronounced as samples are subject to higher axial loads. The analytical model satisfies the relationship of sample bending satisfactorily with acceptable accuracy.

Muhammad Hadi (2012) submits the investigation of the numerical model was developed and applied to the verification of basic behaviors of the thin-walled high strength of CFST slender beam-column. Use the final experimental load deviation and resistance response of the CFST beam-column tested by independent researchers to examine the accuracy of the numerical model. Use the verified numerical model to investigate the influence of column slender ratio, local buckling, the load eccentricity ratio, the depth-thickness relationship, the strength values of the steel and the concrete compression strengths on the behavior of the model high strength thin-walled CFST slender beam-columns. It is shown that the numerical model is efficient and precision to determine the behavior of thin-walled CFST slender beam-columns of high strength with local buckling effects. Numerical results presented in this studies are beneficial for the expansion of composite design codes for thin-walled, high-strength rectangular CFST slender beam-column.

Yansheng Du (2017) studied, 12 rectangular CFT columns using Q460 grade steel were tested under decentralized load and the experimental results were discussed. To verify the effect of steel strength, width, and thickness, and aspect ratio, the parametric test was performed using verified FEM (nonlinear finite element model (FEM))(H / t) final resistance value computed by AISC-360, EC4-2004, Chinese Code CECS-159. By comparison, high aspect ratio steels with high strength and various h / t ratios were predicted by FEM. The results presented that three design codes are safe in the design of a column with a higher aspect ratio. EC4-2004 was conservative in the design of rectangular CFT columns using high strength steel up to 690 MPa under the limit of h/t ratio. The AISC-360 method can precisely predict the maximum resistance of a rectangular CFT column with a steel strength of 550 Mpa. The method of CECS 159 is very modest and can be safely used up to the strength of steel up to 690 Mpa. Figure 2.2 shows the test setup

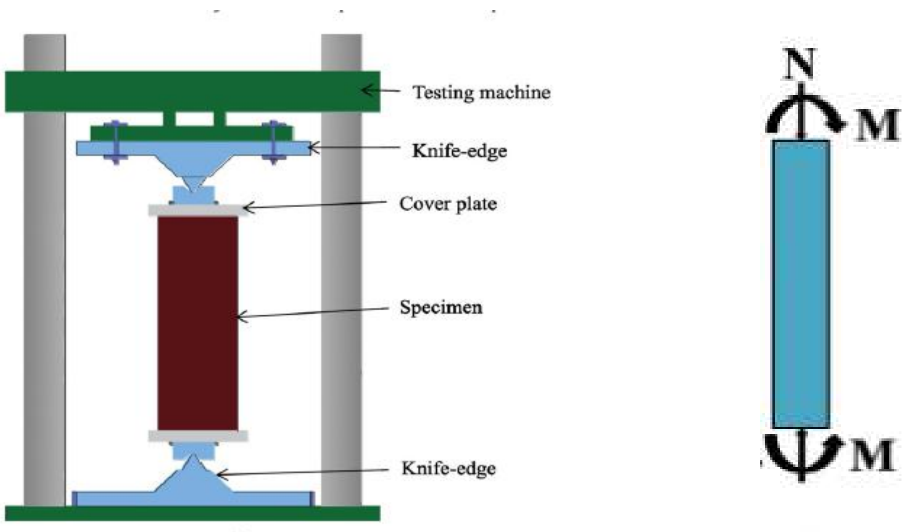

Figure 2.2 The test setups

Thes test results showed that the maximum moment resistance and the axial resistance decrease by 20.9 and 5.7% respectively when the aspect ratio changed from 1.5 to 1.0.

However, as the aspect ratio decreases from 2.0 to 1.5, the resistance does not change much (Yansheng Du *et al.*, 2017).

2.3 Reliability analysis

Naveen Kumar (2017) obtained the reliability analysis and analytical study of steel Tube with concrete filled under the monotonic loading. The analytical results are obtained by the Finite element NASTRAN software are investigated using American Concrete Institute ACI-318-1999 code. Diversity may be found to be 20% range accordingly to the ACI-318-1999 code. Reliability technique is routed under probabilistic variables such as thickness, length, diameters, and the grades of concrete with the percentage of glass fibers. The results gained by using First Order Second Moment Method FOSM for the analysis. A subset simulation was depended on the analysis. The results show that as the diameter increases, the reliability of the member's increases as shown in Figure 2.3. Since the load carrying capacity depends mainly on the strength of concrete, the higher the grade of concrete the better the reliability as shown in Figure 2.4.

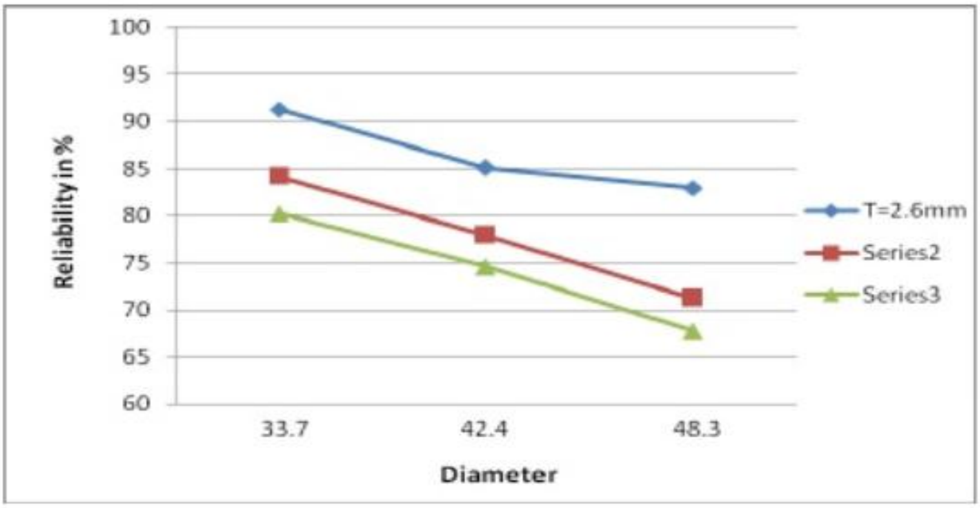

Figure2.3 Reliability vs Diameter

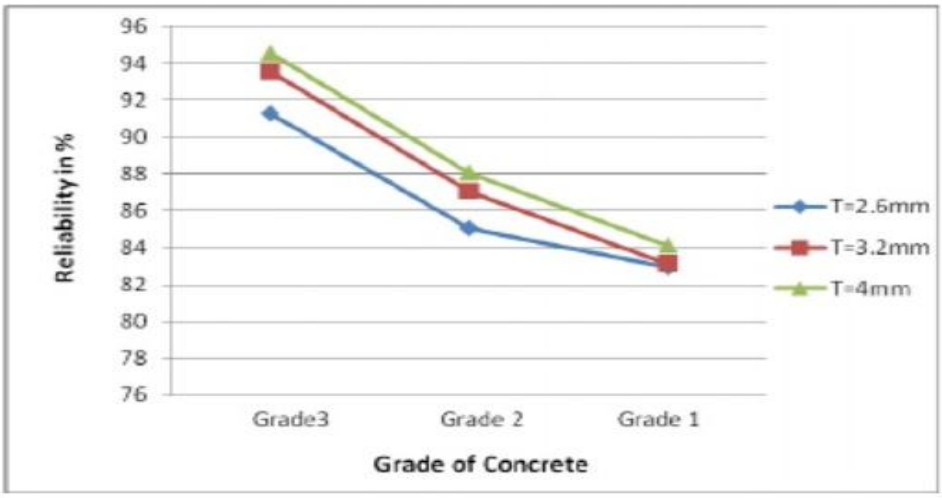

Figure 2.4 Reliability vs grade of concrete with diameter 33.7 mm

Mohammed Bilal (2017) offered reliability analysis and analytical study of hollow steel tubes filled with different grade of concrete under monotonous load was carried out. The nonlinear behavior of the column is recognized using the finite element software ANSYS 16.0. The results of nonlinear finite element analysis have been achieved and demonstrated by American Institute of Steel Construction AISC-LRFD-1999 code and reliability analysis. This study investigated that the influence of many parameters such as steel tube diameter (42.40 mm, 33.70 mm, 26.90 mm), tube thickness 3.2 mm, slenderness ratio, reliability, etc. and evaluated the composite column on the compression response under the axial load. From the results concluded that the obtained Pu values by AISC LFRD code the analytical and formulae procedure presented that the results obtained by the analytical method are higher than those of the coded values, The percentage of error between Pu AISC LFRD method and Pu analysis is about 12%. With increasing in L/d ratio The load carrying capacity of CFST is decreased, but the reliability index β value increases with increasing length of the CFST column with constant thickness and diameter.

Chethan Kumar (2016) studied the reliability analysis of CFST. In reliability analysis, it is defined using the performance function. the capacity of the structure was taken from experimental results which were conducted by CFST. A resistance function of a structure created based on the EC4-2004 specification for composite structures. Next, the reliability of the CFST using the Reliability Index Approach (RIA) such as the Reliability Indicator First Order Reliability Method FORM is implemented. Consider parametric effects on the reliability of CFST. By constructing the research, it is concluded that such parameter variations have a major impact on the structural reliability of CFST. The results show that the procedure of design of CFST columns is Very consistent. It was investigated that the safety level was increasing with increasing of the strength of infill in the tube. It can be concluded the random variance of parameters such as thickness, diameter, and length has significant effects on the structural reliability Figure 2.5 show the relationship between the diameter of CFS column and reliability in percentage. Although this article focuses majorly on estimating the reliability of CFT, the reliability for other composite structures can also be taken by following the same procedure.

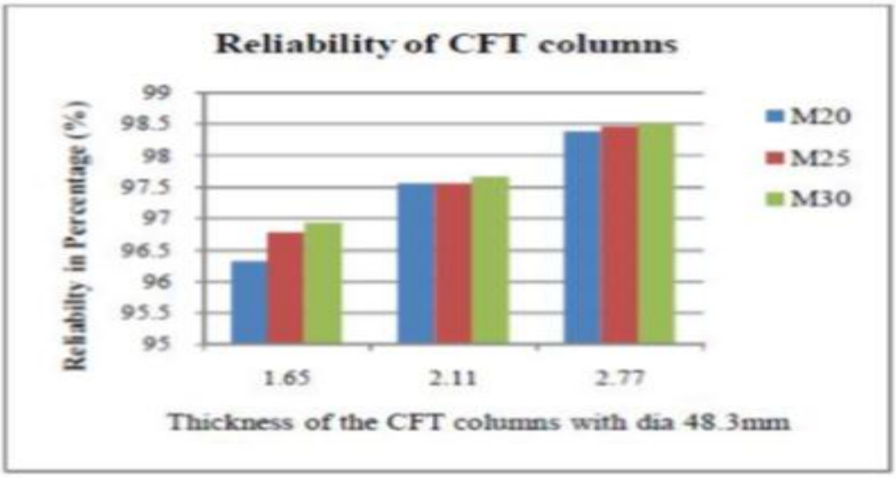

Figure 2.5 Reliability percentage V/S diameter of CFS

Chethan Kumar (2016) presented the reliability of the structure was obtained from the experimental results carried out. A resistance function of a structure created based on Eurocode provisions on composite structures. Next, verify the reliability of CFT using the Monte Carlo Simulation Method. By constructing the study, it is concluded that such parameter variations have a major influence on the structural reliability of CFT. The safety of the design level increasing with increase the grade of the concrete due to the actual that the load was carrying capacity of a designed member is a function of concrete strength. Generally, the safety of the designed section decrease with the increase of the section diameter as shown in Figure 2.6. It can be investigated that the maximum reliability was taken is 96.63 % for T1, D2, and G2 for a constant length, and the maximum combination obtained was T1, D2, and G2 as shown in Figure 2.7.

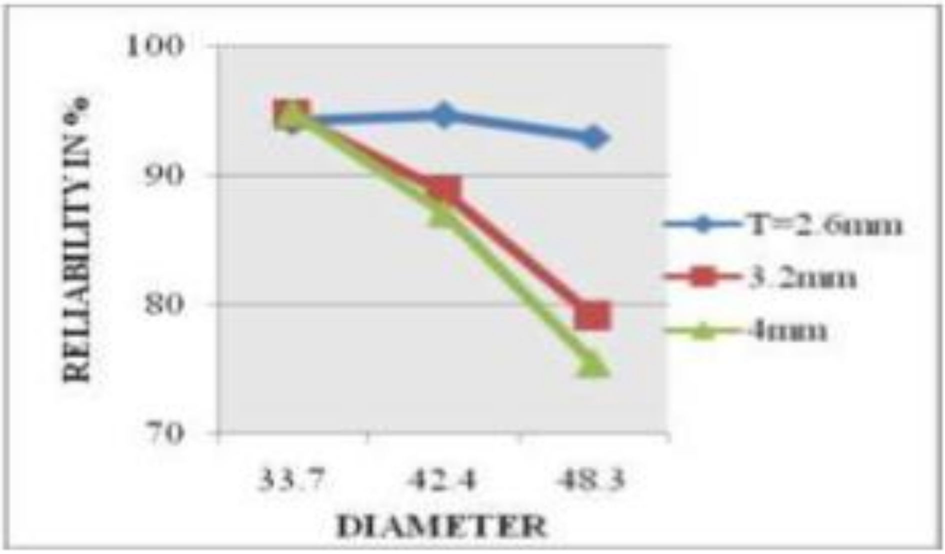

Figure 2.6 Reliability V/S Diameter

Figure 2.7 Reliability V/S Teguchi's array combinatio

CHAPTER 3

METHODOLOGY

3.1 General

In this chapter, the design of composite steel and concrete of Circular Concrete Filled Steel Tube CCFST and, Rectangular Concrete Filled Steel Tube RCFST members explained by AISC-360-10 and EC4-2004. These codes are used in the calculation of the reliability percentage.

As shown in Figure 3.1, we summarize the formulas for calculating the geometric properties (width of steel tube (B), the height of steel tube (H), the thickness of the steel tube (t), the width of concrete (h_i), hethe ight of concrete (b_i), external radius of steel (r_s), internal rthe adius of concrete (r_c), area of steel the tube (A_s), area of concrete fthe ill (A_c), plastic section moduluthe s of concrete (Z_c), plastic section modulus ofthe steel (Z_s), moment of inertia of the concrete (I_c), and moment of inertia of the steel tube (I_s)) of concrete and steel in Table 3.1 with geometric notation. In the case of HSS, the geometrical properties of the steel tube can also be obtained from the manual of EC 4 - 2004 and AISC 360 - 10. Since the formula in Table 3.1 does not consider the fillet radius, there is a slight difference between the moment of inertia and the coefficient of plastic section modulus of a steel tube.

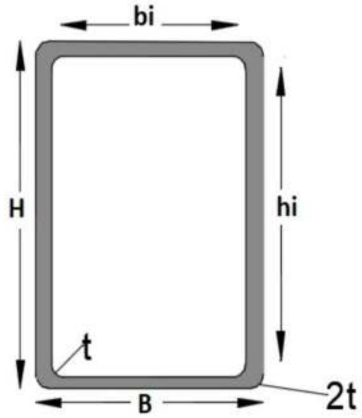

Figure 3.1 Notation in geometric dimensions for RCFST

Table 3.1 Geometric properties for RCFST

Concrete filled tube	Steel tube
$h_i = H - 2t$ $b_i = B - 2t$ $r_c = r_s - t = t$	$r_s \approx 2t$
$A_c = b_i h_i - (4 - \pi)\, r_c{}^2$	$A_s = BH - (4 - \pi)\, r_s{}^2 - A_c$
$Z_s = \frac{bh^2}{4} - Z_c$	$Z_c = \frac{b_c h_c{}^2}{4}$
$I_c = \frac{b_i h_i{}^3}{12}$	$I_s = \frac{BH^3}{12} - I_c$

3.2.Design Steps of AISC360-10 Code for Capacity Estimation for RCFST

There are two methods in AISC360-10 for composite the first one was plastic stress distribution method and the second method is the strain compatibility method. The plastic stress distribution method is the widest method, which provides a simple estimation for the most design situations while the strain compatibility method provides a general calculation method. Plastic stress distribution method used to calculate the nominal strength of the composite section. However, in special cases where the cross-sectional area changes, strain matching method is a better choice.

3.2.1 The limitation of materials for AISC360-10

Steel and concrete in the composite system are subject to the following restrictions.

1- Concrete compressive strength ($f_c{}'$) should be between 21 MPa and 70 MPa, this is for the normal weight concrete case, and between 21 MPa and 42 MPa of lighthe tweight concrete case.
2- Yield in the case of structural steels and reinforcing bars, the minimum yield stress (F_y) should not exceed 525 MPa

3.2.2 The filled composite sections classification for local buckling for RCFST

In the case of compression, the parts of filled composite are classified as non-compact, compact, or slenderness. For compartments which are considered compact, the maximum thickness direction ratio (B/t) of the compressed steel members must not exceed the limit value B/t, λ_p selected in Table 3.2. If one or more of the steel compression members has a maximum B/t greater than λ_p but does not exceed λ_r in Table 3.2, the filled composite part is not compact. When the maximum compression ratio of the compressed steel exceeds λ_r exceeds. The maximum allowable value B/t is the value specified in Table 3.2.

Table 3.2 Width-thickness ratios limitation for compression steel elements in composite members subject to axial compression.

Description of element	Width to thickness ratio	λ_p Compact /Noncompact	λ_r Noncompact/ Slender	Maximum permitted
Walls of rectangular HSS and boxes of uniform thickness	b/t	$2.26\sqrt{\frac{E}{F_y}}$	$3.00\sqrt{\frac{E}{F_y}}$	$5.00\sqrt{\frac{E}{F_y}}$
Round HSS	D/t	$\frac{0.15E}{F_y}$	$\frac{0.19E}{F_y}$	$\frac{0.31E}{F_y}$

In the case of compression, the parts of the filled composite are classified as non-compact, compact, or slenderness. For compartments deemed compact, the maximum B/t shall of the compressed steel element shall not exceed B/t λ_p limiting in Table 3.3. If one or more of the steel compression elements has a maximum B/t greater than λ_p override, but not exceeding the λ_r over in Table 3.3, that part is uncompressed. If the ratio *B/t* of any steel material exceeds λ_r, the cross section is slenderness. The maximum ratio of B/t allowable is as shown in the Table 3.3.

Table 3.3 Width-thickness ratios limitation for compression steel elements in composite members subject to flexure.

Description of element	Width to thickness ratio	λ_p Compact /Noncompact	λ_r Noncompact/ Slender	Maximum permitted
Flanges of rectangular HSS and boxes of uniform thickness	b/t	$2.26\sqrt{\frac{E}{F_y}}$	$3.00\sqrt{\frac{E}{F_y}}$	$5.00\sqrt{\frac{E}{F_y}}$
webs of rectangular HSS and boxes of uniform thickness	h/t	$3.00\sqrt{\frac{E}{F_y}}$	$5.70\sqrt{\frac{E}{F_y}}$	$5.70\sqrt{\frac{E}{F_y}}$
Round HSS	D/t	$\frac{0.09E}{F_y}$	$\frac{0.31E}{F_y}$	$\frac{0.31E}{F_y}$

3.2.3 The axial load and bending moment capacity for CCFST members

The corresponding design code varies from country to country, and the codes do not match each other. Therefore, the calculated value of bending strength and moment capacity when pure bending varies depending on the design code. In this research, we describe ACI, AISC, and Euro code 4 which provides a method for estimating the bending strength of the concrete filling pipe. First, the ACI building code and the AISC-360-10 specification provide design rules for US composite members. The ACI building design code (ACI318-14) contains only one method, but there are two methods for AISC Plastic Stress Distribution Method (PSDM) and Strain Matching Method (SCM). However, the ACI method is conceptually the same as the distortion adaptation method of AISC-LRFD (2011) which is one of the two methods included in AISC. The ACI method is implemented by considering CFT as a normal reinforced concrete and replacing rebar with the same amount of rebar. The moment capacity of the CFT beam is calculated based on the assumption of a concrete compressive strain of 0.003. Furthermore, according to ACI 318-14 Section 22.2.2.3, the relationship between concrete compressive stress distribution and concrete strain can be assumed in several forms such as rectangles and trapezoids. There are various ways to assume the relationship between compressive stress distribution of concrete and strain, but since this research is the most general assumption, we will deal with only the rectangular compressive stress distribution of concrete. Therefore, in this study, the compressive strength of concrete is equivalent rectangular stress distribution, and its value is assumed to be 0.85 fc' Whitney rectangular stress distribution. Here, f'c' is the compressive strength of concrete. The depth of the concrete equivalent stress block a, is the same as β_{1c} , but the tensile strength of the concrete is ignored, β_1 is the Whitney stress block depth coefficient, c is the neutral axial depth from the extremely compressed fiber is there. In the case of steel, it is assumed to follow a completely elasto-plastic stress-strain relationship, and it has a perfectly coupled state between steel pipe and concrete. AISC suggests two methods. PSDM is another method proposed by AISC and is different from ACthe I method or AISC SCM. PSDM is a simplified version of SCM and calculates section strength based on plastic stress distribution. The concrete compressive stress in the plastic state of a circular concrete filling tube is assumed to be a uniform stress of 0.95 f'c. As mentioned above, in the ACI method, it is assumed that the compressive uniform stress of concrete is 0.85 f'c, and in practice AISC also imposes the same assumptions for a Rectangular Concrete Filling Tube RCFT. However, because AISC's PSDM takes into account the confinement due to the hoop stress in the circular pipe, a coefficient of 0.95 is used for the uniform stress of the Circular Concrete Filled Steel Tube CCFT concrete. The depth of the concrete equivalent stress block is equal to the distance from the extremely compressed fiber of the concrete to the neutral axis (different from the depth of the Whitney stress block). In particular, only the PSDM of AISC provides the formula for calculating the flexural strength of the CCFT, and its expression is expressed as follows (AISC 2011). In the case of CCFT, the moment capacity Mn or M used in AISC

$$M_B = fyZsB + \frac{0.95fc'ZcB}{2} \tag{3.1}$$

Where F_y, Z_{sB}, f'_c, and Z_{cB} denote the yield strength of steel tube, the plastic section modulus of steel tube at point B where no axial force is applied to the CCFT, the compressive strength of concrete, and the plastic section modulus of concrete at point B, respectively. Here, Z_{sB} and Z_{cB} are also provided as follows:

$$Z_{sB} = \frac{d^3 - h^3}{6} \sin\frac{\emptyset}{2} \tag{3.2}$$

$$Z_{cB} = \frac{h^3 \sin^3\frac{\emptyset}{2}}{6} \tag{3.3}$$

Where

$$\emptyset = \frac{0.0260 - 2K_s}{0.0848K_c} + \frac{\sqrt{(0.0260K_c + 2K_s)^2 + 0.857K_cK_s}}{0.0848K_c} \tag{3.4}$$

Where d is the outer diameter of the Circular Concrete Filled Tube CCFT, his the diameter of the concrete section or inner diameter of the steel tube, and θ is the angle that defines the location of the plastic neutral axis at the inner face of the steel as shown in Figure 3.2

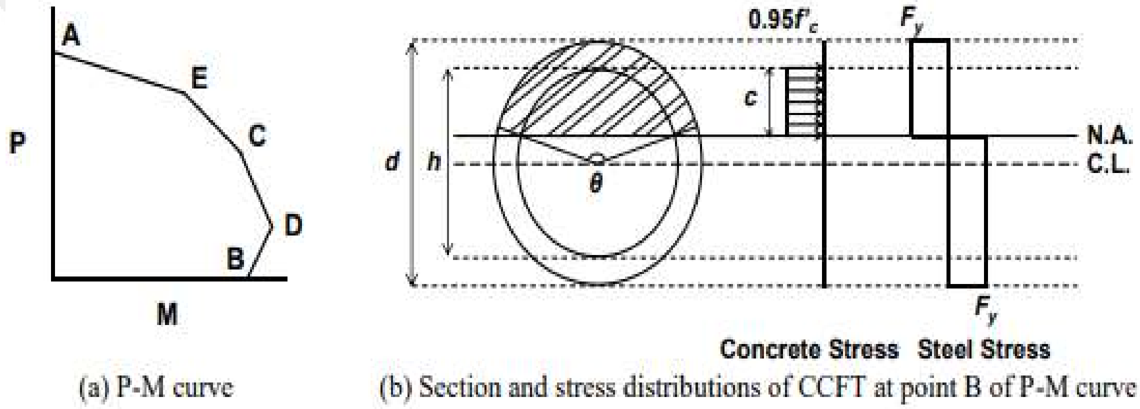

Figure 3.2 Section and stress distribution of CCFST at point B of the P-M curve the figure adopted from and applied by AISC 2011 (Minsun Lee and Kang, 2016)

Where

$$K_c = f_c h^2 \tag{3.5}$$

$$K_s = f_y\left(\frac{d - t}{2}\right)t \tag{3.6}$$

Using these equations, the manual calculation to estimate the bending strength of Circular Concrete Filled Tube CCFT is only possible in Plastic Stress Distribution Method PSDM of AISC. However, since PSDM permits errors in the process of deriving the plastic section modulus of concrete and steel at point B, the bending capacity according to the equation in PSDM of AISC is not accurate and is approximate to CCFT (Geschwindner 2010) is there. The degree of approximation becomes larger for thick-walled CCFT. Eurocode 4 can calculate the capacity of the concrete filling tube with two methods strain matching method (SCM) and plastic stress distribution method (PSDM)), a general method like AISC and a simplified method will be used. However, SCM of Eurocode 4 is different from the ACM method and SCM of AISC, but PSDM of Eurocode 4 is also different from PSDM of AISC. Eurocode 2 According to section 3.1.7, like the ACI method and the SCM of AISC, the stress-strain relation of concrete can be assumed in three forms, parabolic, trapezoidal, or rectangular. However, since this study is the most common and convenient assumption, we use only the shape perpendicular to the stress distribution of concrete. In the SCM of Eurocode 4, the final compressive strain, uniform compressive stress, and depth of equivalent rectangular stress distribution are different depending on the strength of the concrete. For example, if the concrete strength is 27 MPa, the final compressive strain of the concrete is 0.0035, the uniform compressive stress is f'c, the equivalent rectangular stress distribution depth is 0.8 c, concrete Is 60 MPa, the final compressive strain of the concrete is 0.0029, the uniform compressive stress is 0.95 f'c, and the depth of the equivalent rectangular stress distribution is 0.775 c. Regarding tension, like the ACI method or the SCM of AISC, the tensile strength of concrete is ignored and it is assumed that the steel is completely elastic-plastic. Eurocode 4's PSDM has some aspects that are common or different from AISC's PSDM. Because Eurocode 4's PSDM uses rigid plasticity analysis just like AISC's PSDM, moment capacity is obtained on the premise that there is a complete interaction between steel and concrete. The compressive stress distribution of concrete is assumed to have an equivalent rectangular stress distribution. The value is f'c, which is different from the value of AISC's PSDM, its depth again being the distance from the extreme compression fiber to the neutral axis.

3.2.3 The Axial Load For Columns For RCFST

The permissible compressive strength, P_n/Ω_c, and design compressive strength $\emptyset_c P_n$, for axial load filled composite columns must be calculated for the limiting state of bending buckling based on member slenderness as follows:

The AISC360-10 code specification for determining the ultimate load (P_n) of a RCFST column is given by Eqs. (3.7) and (3.8).

The Load Resistance Factor Design (LRFD) $\phi_c = 0.75$ and the allowable Stress Design (ASD) $\Omega_c = 2.00$

(a) When $\frac{P_{no}}{P_e} \leq 2.25$ $\qquad P_n = P_{no}\left[0.658^{\frac{Pno}{Pe}}\right]$ (3.7)

(b) When $\frac{P_{no}}{\mathrm{Pe}} > 2.25$ $\qquad P_n = 0.877P_e$ (3.8)

Where the P_n is nominal axial strength (N), P_{no} is nominal compressive strength of zero length (N), and the (P_e) is elastic critical buckling load (N) can be calculated according to Euler's formula, of the AISC360-10 code as shown in Eq. (3.9).

$$P_e = \frac{\pi^2\left(EI_{eff}\right)}{(kL)^2} \qquad (3.9)$$

Where k is effective length factor and it is as shown in Table 3.4 and L is laterally unbraced length of the member (mm).

$$EI_{eff} = C_1E_cI_c + E_sI_s \qquad (3.10)$$

Where Ec is mothe dulus of elasticity of concrete (0.043wc 1.5 $\sqrt{f_c'}$, MPa), w_c is weight of concrete per unit volume ($1500 \leq w_c \leq 2500$, kg/m^3), I_c is moment of inertia of concrete (mm^4), $C_1$is coefficient for calculation of effective rigidity of an encased composite compression member Eq. (3.11), E_s is modulus of elasticity of the steel (200000 MPa), and $I_s$is moment of inertia of the steel (mm4).

$$C_1 = 0.1 + 2\left(\frac{A_s}{A_c + A_s}\right) \leq 0.3 \qquad (3.11)$$

Where A_s is the cross-sectional area of steel section (mm^2) and A_c is the cross-sectional area of concrete (mm^2).

The effective stiffness of the composite section EI_{eff} ($N.mm$2) is determined from Eq. (3.10).

Table 3.4 The Approximate Values of The Effective Length Factor, K

Buckled shape of column shown by dashed line	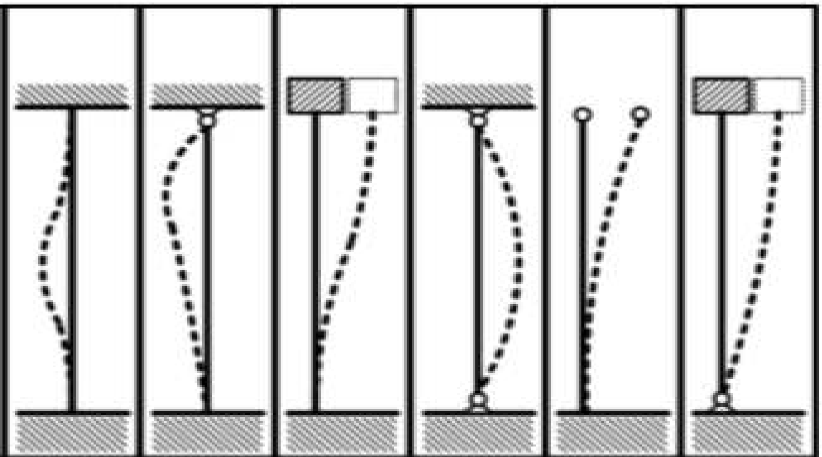					
Theoretical K value	0.5	0.7	1.0	1.0	2.0	2.0
Recommended design value K	0.65	0.80	1.2	1.0	2.10	2.0
End condition key	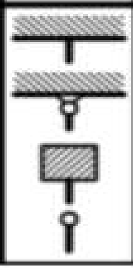	Rotation fixed and translation fixed Rotation free and translation fixed Rotation fixed and translation free Rotation free and translation free				

Figure 3.3 shows the graphic representation of the nominal axial compressive strength of zero length (p_{n0}) for compa osite section of Hollow Steel Section (HSS) slenderness. As shown in Figure 3.3, the compact section complete plastic nominal bearing strength (p_p) can be expressed at the time of compression. The nominal axis direction the intensity p_{no} of the non-compact section can be found using quadratic interpolation between the plastic strength p_p and the axial yield strength (p_y) tube slenderness. This interpolation is secondary.

The capacity of the steel tube includes concrete filling subject to inelastic and volume expansion. It decreases rapidly with the HSS. The slender section is limited to development paramount buckling resistance of steel HSS critical stress infill (F_{cr}) and $0.70f_c{}'$of concrete infil

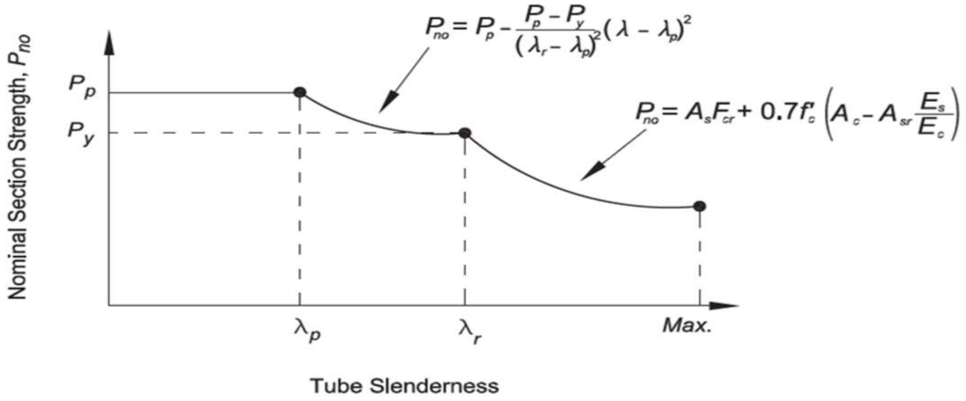

Figure 3.3 Nominal axial strength, p_{n0} versus HSS slenderness ($B\ t/$) (Lai, Varma and Zhang, 2014)

a) Non-Compact Sections

In the case of non-compact section ($\lambda_p \leq \lambda \leq \lambda_r$), the nominal compressive strength of zero length (p_{no}) of an axially loaded of RCFST can be calculated from Eqs. (3.12), (3.13) and (3.14).

$$p_{no} \ = p_p - \frac{p_p - p_y}{\left(\lambda - \lambda_p\right)^2}\left(\lambda - \lambda_p\right)^2 \quad (3.12)$$

$$p_p = f_y A_s + 0.85 f_c{}' A_c \quad (3.13)$$

$$p_y = f_y A_s + 0.7 f_c{}' A_c \quad (3.14)$$

b) Compact Sections

For the case of a compact section ($\lambda \leq \lambda_p$), the nominal compressive strength of zero length (p_{no}) of an axially loaded of RCFST can be determined with the limit state of flexural buckling as shown in Eq. (3.15).

$$p_{no} = p_p = f_y\ A_s + 0.85\ fc'Ac \quad (3.15)$$

c) Slender Sections

The case of slender section ($\lambda_r \leq \lambda \leq \lambda max$), the nominal compressive strength of zero length (p_{no}) of an axially loaded of RCFST can be determined from Eq. (3.16).

$$p_{no} \ = F_{cr}\ A_s + \ 0.7 fc'Ac \quad (3.16)$$

$$F_{cr} = \frac{9\ E_s}{\left(\frac{b}{t}\right)^2} \quad (3.17)$$

The effective stiffness of the composite section (EI_{eff}) can be estimated for all parts using the following Eq. (3.18).

$$EI_{eff} = C_3 E_c I_c + E_s I_s \tag{3.18}$$

Where C_3 is the coefficient for evaluation of effective rigidity of the filled composite compression member, is estimated from Eq. (3.19).

$$C_3 = 0.6 + 2\left(\frac{A_s}{A_c + A_s}\right) \tag{3.19}$$

3.2.5 The Bending moment capacities (beams) for RCFST

If ($\lambda \leq \lambda_p$) compact section. Distance of neutral axis (a_p) from the compression face is evaluated by establishing axial force equilibrium over the crosssection, the plastic moment strength (M_p), and the nominal flexural strength (M_n). The Eqs. (3.14) and (3.15) for evaluating a_p and $M_p$are used. The variables of these equations are Appears in Figure 3.4. In these equations b, H,t_f, t_w are the width, tube depth, flange thickness, and web thickness respectively. .

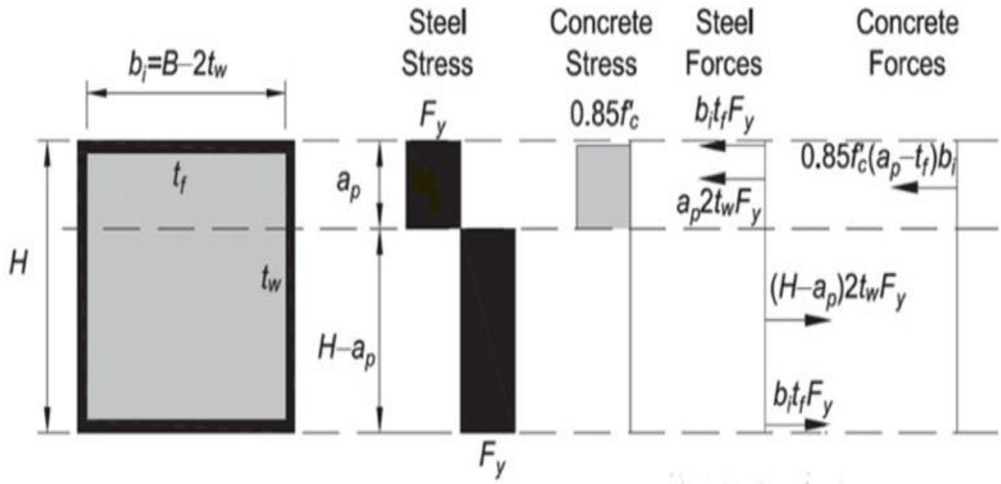

Figure 3.4 Compact section-stress blocks for calculating M_p (Lai, Varma and Zhang, 2014)

$$a_p = \frac{2F_y H t_w + 0.85fc' b_i t_f}{4t_w F_y + 0.85fc' b_i} \tag{3.20}$$

$$M_n = M_p = F_y b t_f \left(a_p - \frac{t_f}{2}\right) + F_y b_i t_f \left(H - a_p - \frac{t_f}{2}\right) + F_y a_p 2t_w \left(\frac{a_p}{2}\right)$$

$$+F_y(H - a_p)2t_w \left(\frac{H - a_p}{2}\right)$$

$$+ 0.85f'_c(a_p - t_f)b\left(\frac{a_p - t_f}{2}\right) \; for\; \lambda \le \lambda_p \quad (3.21)$$

The non-compact section ($\lambda_p \le \lambda \le \lambda_r$) Figure 3.4. As shown, to evaluate the minimum binding capacity of non-compact sections with tube slenderness (λ) =λ_r. Distance of the neutral axis (a_y) from the compression plane is evaluated by establishing axial force balance over the cross section, and the moment capacity (M_n=M_y) is estimated using this neutral axis location as shown in Eqs. (3.16) and (3.17) for calculating(a_y) and M_y are shown in Figure 3.5.

$$a_p = \frac{2F_y H t_w + 0.35fc' b_i t_f}{4t_w F_y + 0.35fc' b_i} \quad (3.22)$$

$$M_n = M_P = F_y b_i t_f \left(a_y - \frac{t_f}{2}\right) + F_y b_i t_f \left(H - a_p - \frac{t_f}{2}\right) + 0.5F_y a_y 2t_w \left(\frac{2a_y}{3}\right)$$

$$+ 0.5F_y(H - a_y)2t_w \left(\frac{2(H - a_p)}{3}\right)$$

$$+ 0.35fc'(a_y - t_f)b\left(\frac{2(a_y - t_f)}{3}\right) \quad (3.23)$$

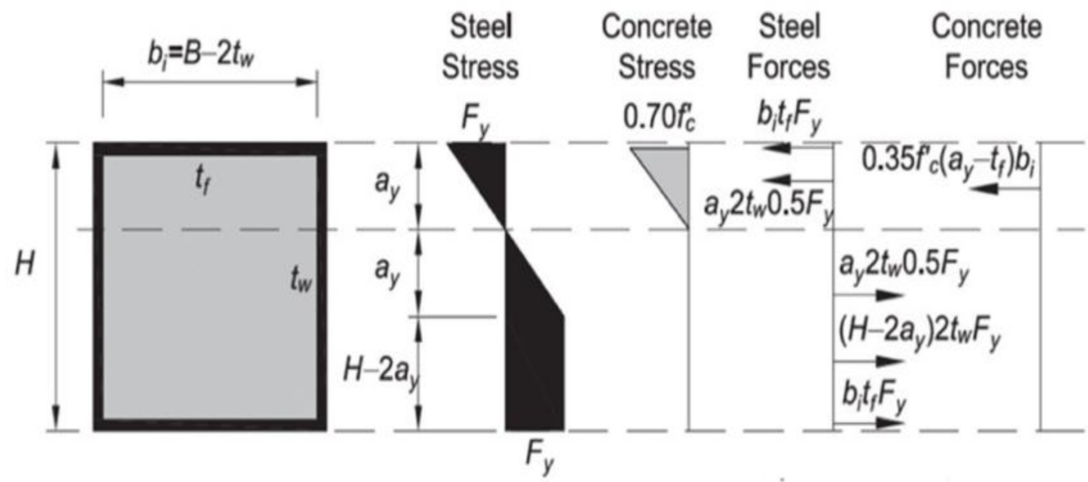

Figure 3.5 Noncompact section-stress blocks for calculating M_y (Lai, Varma and Zhang, 2014)

The nominal moment capacity $M_n$can be calculated using Eq. (3.24).

$$M_n = M_p - \frac{(M_p - M_y)(\lambda - \lambda_p)}{\lambda_r - \lambda_\mathrm{p}} \;\; for\ \lambda_p < \lambda \leq \lambda_r \tag{3.24}$$

Figure 3.6 shows the change in nominal bending strength(M_n) of the filling HSS slender section. As described, the complete plastic deflection strength (M_p), the non-compact nominal bending strength (M_n) for the sections can be evaluated using linear interpolation between plastics strength (M_p) moment at yield strength (M_y) HSS slenderness. The slender section are limited in order to development the first yield moment (M_{cr}) of the composite part the tension flange first contracts and the compression flange. It is limited to the critical buckling strength,F_{cr} and the concrete is limited to linear elasticity behavior with maximum compressive stress it is equal to $0.70 f_c$ '

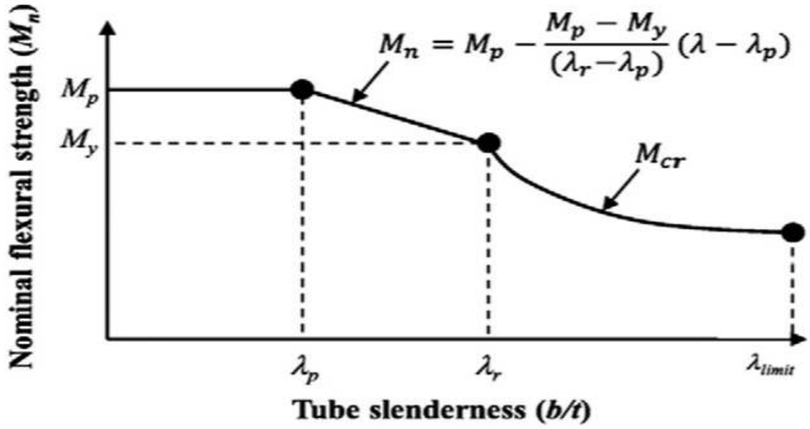

Figure 3.6 The nominal bending moment capacity of filled beam versus HSS slenderness (Lai, Varma and Zhang, 2014)

Slender section ($\lambda_r \leq \lambda \leq \lambda_{max}$) estimate the minimum bending capacity of the slender sections as appears in Figure 3.7. Eqs. (3.19) and (3.20). The distance of the neutral axis (a_{cr}) from the compression face is estimated by establishing axial force balance over the cross-section, and the moment capacity (M_n=M_{cr}). The variables of these equations are graphically defined in Figure 3.7.

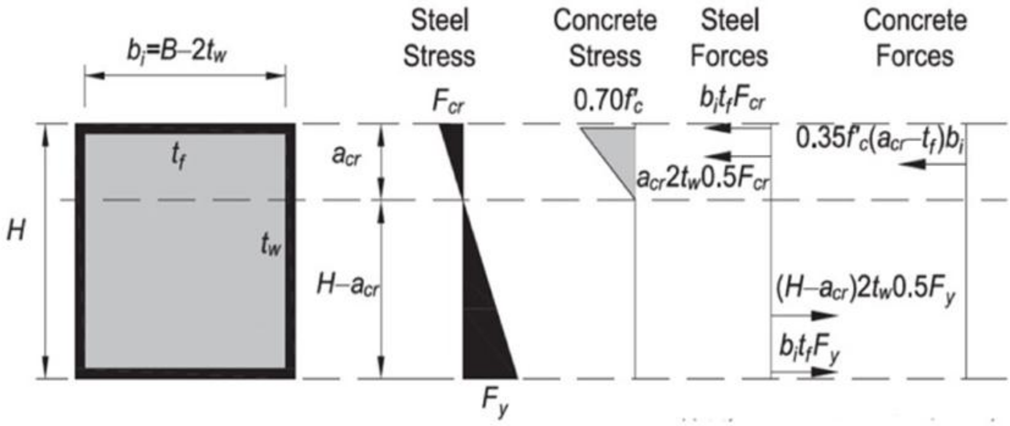

Figure 3.7 Slender section-stress blocks for calculating first yield moment, M_{cr} (Lai, Varma and Zhang, 2014)

$$a_{cr} = F_y H t_w + \frac{(0.35fc' + F_y - F_{cr})b_i t_f}{t_w(F_{cr} + F_y) + 0.35fc' b_i} \tag{3.25}$$

$$\begin{aligned} Mn = Mp = {} & \mathrm{F_{cr} b_i t_f}\left(\mathrm{a_{cr}} - \frac{\mathrm{t_f}}{2}\right) + \mathrm{F_y b_i t_f}\left(H - \mathrm{a_{cr}} - \frac{\mathrm{t_f}}{2}\right) + 0.5\mathrm{F_{cr}} 2\mathrm{t_w}\, \mathrm{a_{cr}}\left(\frac{2\mathrm{a_{cr}}}{3}\right) \\ & + 0.5\mathrm{F_{cr}}(H - \mathrm{a_{cr}})2\mathrm{t_w}\left(\frac{2(H - \mathrm{a_{cr}})}{3}\right) \\ & + 0.35fc'(\mathrm{a_{cr}} \\ & - \mathrm{t_f})b\left(\frac{2(\mathrm{a_{cr}} - \mathrm{t_f})}{3}\right) \end{aligned} \tag{3.26}$$

3.2 Combined flexure and axial force (beam-columns)

Interaction curves as illustrated in Figure3.8 from the plastic stress distribution model are shown in Table 3.5 evaluated and applied to each point.

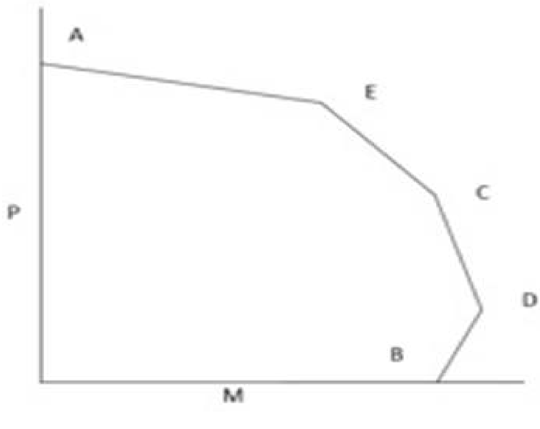

Figure 3.8 Filled rectangular HSS, strong-axis anchor points (AISC360-10)

Table 3.5 Plastic capacities for composite filled HSS bent about either principal axis

Section and stress Distrubution	Pt.	Defining Equations
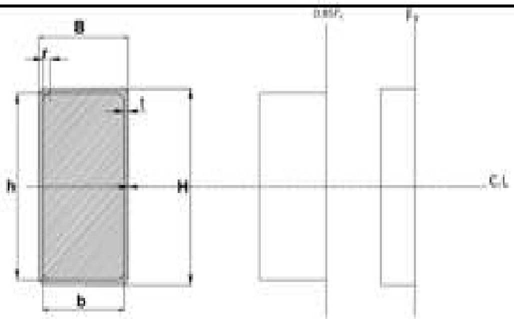	A	$PA = FyAs + 0.85\,fc'Ac$ $MA = 0$ $t = r$ $Ac = bihi - 0.858r^2$ $bi = B - 2t$ $hi = H - 2t$
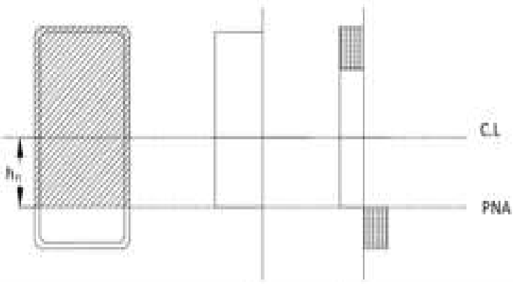	C	$Pc = 0.85fc'Ac$ $Mc = MB$
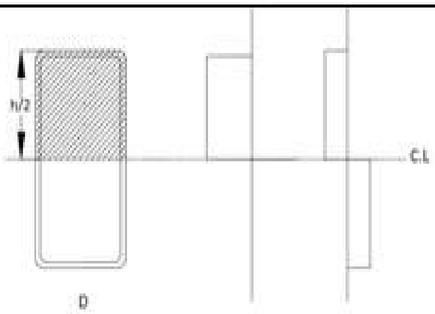	D	$PD = \dfrac{0.85fc'Ac}{2}$ $MD = FyZs + \dfrac{0.85fc'Zc}{2}$ $Zs = \dfrac{bihi^2}{4} + 0.192r^3$
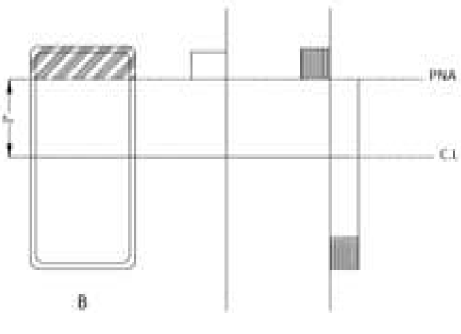	B	$PB = 0$ $MB = MD - FyZsn - \dfrac{0.85fc'Zcn}{2}$ $Zsn = 2thn^2$ $Zc = bihn^2$ $hn = \dfrac{0.85fc'Ac}{2[0.85fc'bi + 4tFy]} \le \dfrac{hi}{2}$
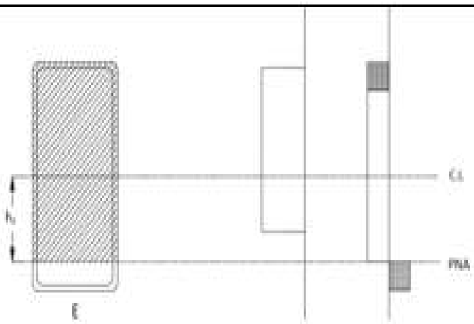	E	$PE = \dfrac{0.85fc'Ac}{2} + 0.85fc'bihE + 4FythE$ $ME = MD - FyZsE - \dfrac{0.85fc'ZcE}{2}$ $ZcE = bihE^2$ $ZsE = 2thE^2$ $hE = \dfrac{hn}{2} + \dfrac{H}{4}$

3.3 Euro Code EC4-2004

There are two methods adopted by the EC4-2004 for evaluating the bending moment capacities and an axial load of a composite member, the general method and the simplified method. In this research, the simplified method was applied. The simplified methods are limited to symmetrical cross section members of CFST and uniform cross sections. When there are two or more unconnected parts in the structural steel, the simplified method is not applied. Implicitness of elements considered implicitly.

3.3.1 The limitations of EC4-2004

1- The axial reinforcement that can be used for evaluations shall not over 6% of the concrete cross section area.

2-The section depth-width h/b ratio of the composite cross section must be within the range of 0.2 and 5.0.

3-Maximum the non-dimensional slenderness ratio of the composite member's λ is limited to 2.0.

Table 3.6 The maximum values (d/t), (h/t) and (b/t_f) with fy in N/mm2

Cross- section	Max(d/t),max(h/t) and max (b/t)
Circular hollow steel sections 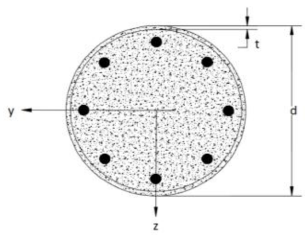	$\max(d/t) = 90\frac{235}{f_y}$
Rectangular hollow steel section 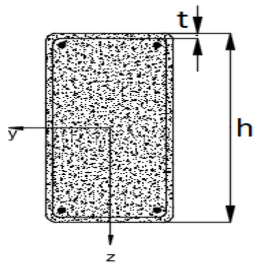	$\max(h/t) = 52\sqrt{\frac{235}{f_y}}$

3.3.2 The combined compression and bending (beam-columns)

The resistance of the composite member subjected to composite compression and bending is determined from the interaction curve illustrated in Figure 3.9

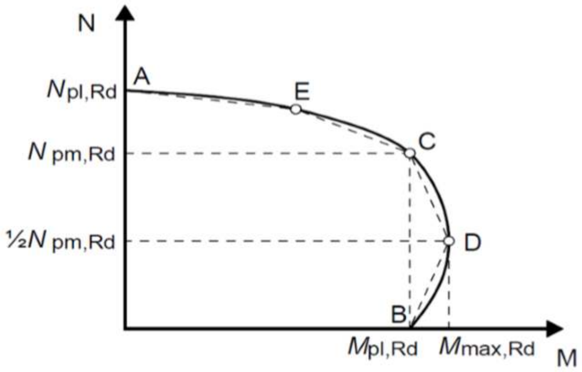

Figure 3.9 Corresponding stress distributions and The interaction curve (Twilt et al. 1994)

In the Figure 3.10, point (A) is the plastic resistance of the cross-section against compression when no bending moment is applied as illustrated in the figure mentioned above. The final axial compressive strength of the formula CFST column and the compressed normal force (N_{PL}) at Eq. (3.27) were evaluated.

$$N_A = N_{PL,Rd} = A_c f_{cd} + A_a f_{yd} \quad (kN) \tag{3.27}$$

Where A_c is the cross-sectional area of concrete, A_a is the cross-sectional area of the structural steel section, f_c is concrete strena gth, and f_y is value of the yield strength of structure steel.

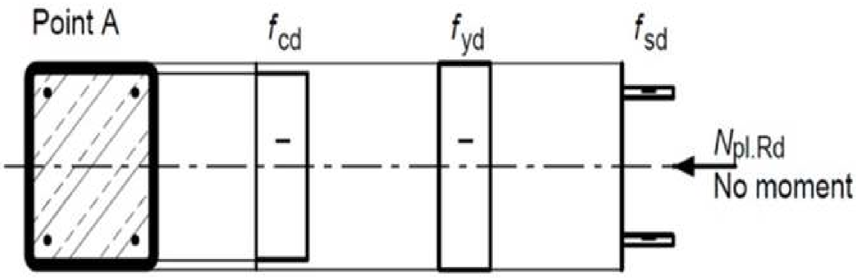

Figure 3.10 The distribution of stress with point (A) on the interaction curve of the concrete filled hollow cross section at $M_A = 0$ (Twilt et al. 1994)

Point (B) as illustrated in the Figure 2, corresponds to the plastic moment resistance of the cross-section can be evaluated from Eq. (3.288) when no axial load is applied as illustrated in Figure 3.11.

$$M_B = M_n = f_y(W_{pa} - W_{pan}) + 0.5f_c(W_{pc} - W_{pcn}) + f_s(W_{ps} - W_{psn}) \quad (3.28)$$

Where u is the ultimate moment, where, f_y, f_s, are the yield strength of the steel and reinforcement, respectively. f_c is the concrete compressive strength, W_{pa} , W_{pc} , and W_{ps} is the plastic section moduli for steel section, concrete, and the reinforcement, and W_{pan} , W_{pcn} , and W_{psn} the plastic section moduli of the section distance 2h from the neutral axis.

In the case of the rectangular hollow section the Wpc can be determine as:

$$W_{pc} = \frac{(b-2t)(h-2t)^2}{4} - \frac{2}{3}\,\mathrm{r}3 - \mathrm{r}2(4 - \pi)\left[\frac{h}{2} - \mathrm{t} - \mathrm{r}\right] - W_{ps} \quad (3.29)$$

Where r is the internal radius of the corners to the hollow section

In case of circular hollow sectionsthe W_{pc} can be calculated in Eq. (3.30);

$$W_{pc} = \frac{(d - 2t)^3}{6} - W_{pc} \quad (3.30)$$

Eq. (3.31) used for both types of sections (rectangular and circular).

$$h_n = \frac{A_c\, f_{cd} + f_{cd}}{2bf_{cd} + 4t(2f_{yd} - f_{cd})} \quad (3.31)$$

For the rectangular hollow sections, it can explain explicitly stated that by Eqs. (3.32) and (3.33).

$$W_{pan} = 2t\, {h_n}^2 \quad (3.32)$$

$$W_{pcn} = (b - 2t)\, {h_n}^2 - W_{psn} \quad (3.33)$$

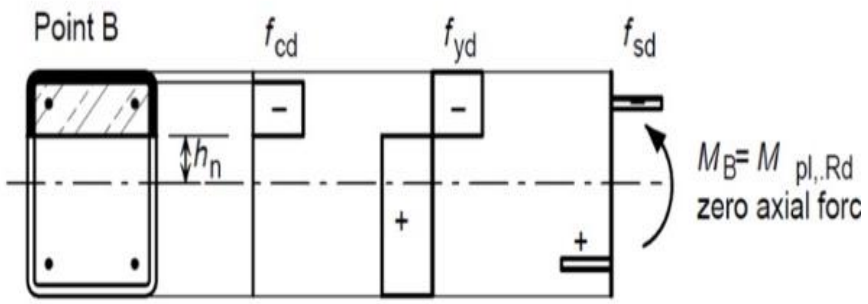

Figure 3.11 The distribution of the stress at point (B) on the interaction curve of concrete filled a hollow cross section at N_b= 0 (Twilt et al. 1994).

At the point (C) as illustrated in Figure 3.12, the axial compression and moment resistance of the composite column is taken as Eq. (3.34)and (3.35), respectively.

$$N_c = N_{Pm,Rd} \; or \; N_{Nc,Rd} = A_c f_{cd} \quad (3.34)$$

$$M_c = M_{pl,Rd} \quad (3.35)$$

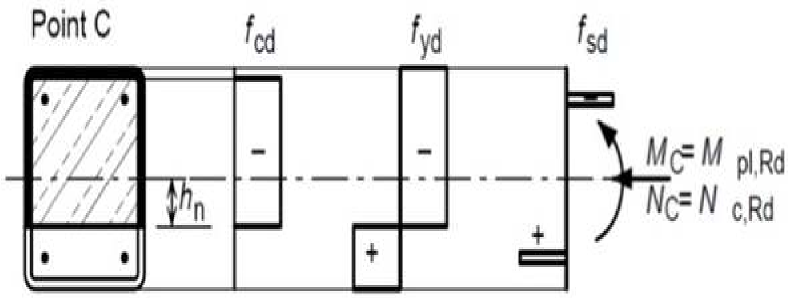

Figure 3.12 The distribution of stress with point (C) on the interaction curve of concrete filled hollow cross section (Twilt et al. 1994).

As shown in Figure 3.13 point (D), the plastic neutral axis coincides with the center of gravity of the cross section, and the resulting axial force is half of the value at point C.

$$N_D = \frac{N_{Pm,Rd}}{2} = M_{max,Rd} = M_D$$

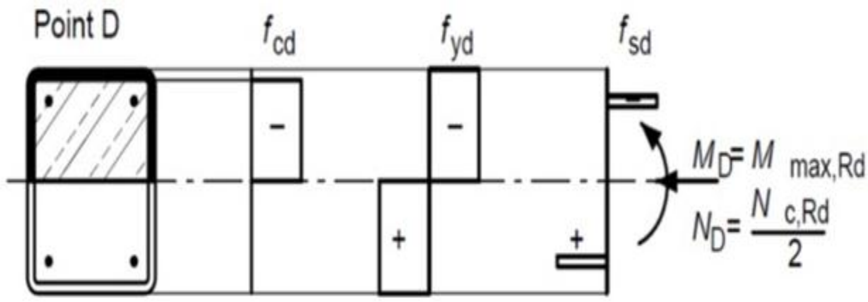

Figure 3.13 The distribution of stress with point (D) on the interaction curve of concrete filled hollow cross section (Twilt et al. 1994).

3.4 Reliability analysis

3.4.1 Risk and Safety Factors Concept

The most basic standard in the design of the structure is to make sure that the strength of the structure is greater than the impact of the applied load. It is well known that geotechnical engineering is related to many uncertain parameters mainly because of the soil fluctuations.

The aim of design based on risk and reliability is to incorporate information on uncertainty into actual problems.

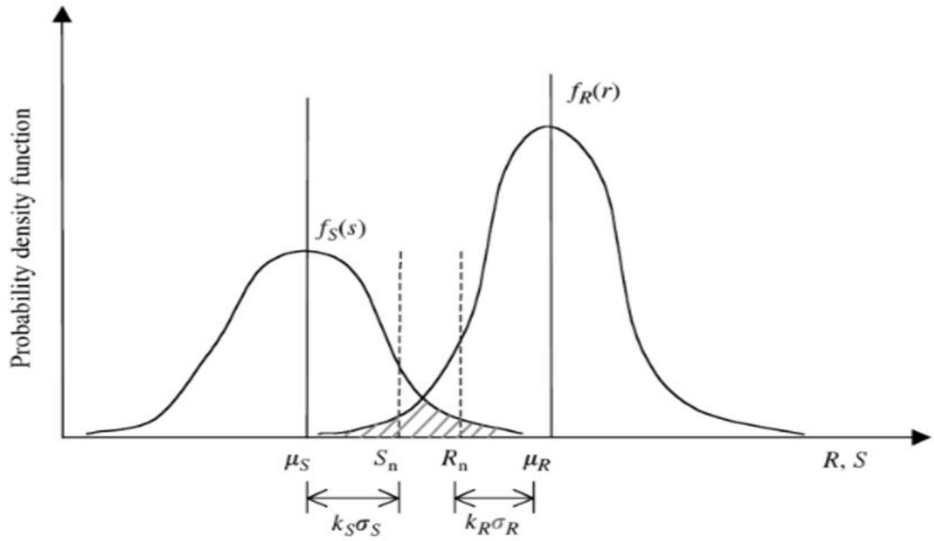

Figure 3.14 Risk assessment basics (Manoj, 2016)

Figure 3.14 is a simple case considering the two variables S and R is referred to the structural load and the resistance of the structure. S and R are random variables and have stochastic properties. These random variables are known as their probability density function and statistical parameters are used to characterize their randomness μ_S and μ_R are probability density functions corresponding to the average value, σ_s and σ_R, their standard deviations and f_s (s) and f_R (s) their corresponding probability density functions. Referring to the Figure 3.14, the deterministic approach ensures the safety of the design by requiring that the RN be greater than the SN with the specified safety margin.

The Nominal $SF = {}^{RN}/_{SN}$ (3.36)

SF is a safety factor. In a definitive design, the uncertainties of all parameters are taken into account by a single number or safety factor. There are different approaches or methods that can be applied based on how the safety factor is applied, ie load, resistance, or both.

- Work stress method: Safety factor applied only to resistance
- Ultimate Strength Method: Safety Factor Applied Only to Load

- ❖ Concrete or Steel (LRDF): Safety Coefficients Applied to Both Resistance and Load Haldar and Mahadevan explain the purpose of these traditional approaches, taking into account the overlap area of the two curves.

This overlapping region provides a qualitative measure of the probability of failure. The extent of overlap depends on the following factors

1. The average of the input parameters is a measure of the relative position of the curve. The longer the distance between curves, the smaller the overlap area and the lower the possibility of failure.
2. The standard deviation is a measure of the variance of the curve. If the width of the curve is narrow, the overlap area will be small and the failure probability will be low.
3. The probability density function is a measure of the shape of a curve. The shape of the curve plays a role in the overlapping region.

To ensure safety in a deterministic design, select the design variable in the area that does not overlap. The safety factor is used to move the position of the curve. However, with such a design, not all overlapping factors are taken into account. The risk-based design is a more reasonable approach because it minimizes overlapping areas considering all design variables to achieve an acceptable level of risk. From the perspective of failure probability, the risk can be defined as follows:

$$pf = (failure) = P(R < S) = \int_0^{\infty}[\int_0^{R} f_R(r)dr\,]f_S(s)\;ds = \int_0^{\infty} \mathrm{F_R(s)\,f_s(s)\,ds} \qquad (3.37)$$

3.4.2 Basic Concepts of Reliability Analysis

The reliability of an engineering design is the probability of meeting a specific requirement under certain conditions. In this research, the CFST member is used to explain this. For stability of the members, it should be designed to satisfy specific requirements for the vertical load. In order for the member to become stable, the supporting force (R) of the CFST must exceed the total vertical load (S) acting on it. Mathematically, this can be expressed as R> S. This is mathematical.

$$\mathrm{Z\ =\ R - S} \qquad (3.38)$$

Where Z appears as a function or a critical state function of the CFST member. This function distinguishes between unsafe zones and safe zones with respect to R and S.

This example has two random variables R and S. This equation can be written as follows;

$\boldsymbol{Z} = (\boldsymbol{x})$

Here g(x) constitutes the n basic variables $x_1, x_2 \ldots . x_n$ of the performance function. Performance functions are based on the fact that it is a measure of the performance of any structure. As any mathematical equation, the function of the lesion can produce three results:

- $g(x) > 0$: Secure region
- $g(x) = 0$: Limit state
- $g(x) < 0$: Failure region

In Figure 3.15 the curve is a performance function. The area to the right of the curve is not safe. However, the area to the left of the curve is a safe area (g (X)> 0). Boundaries or curves represent combinations of variables that are faulty, ie, in a limit state.

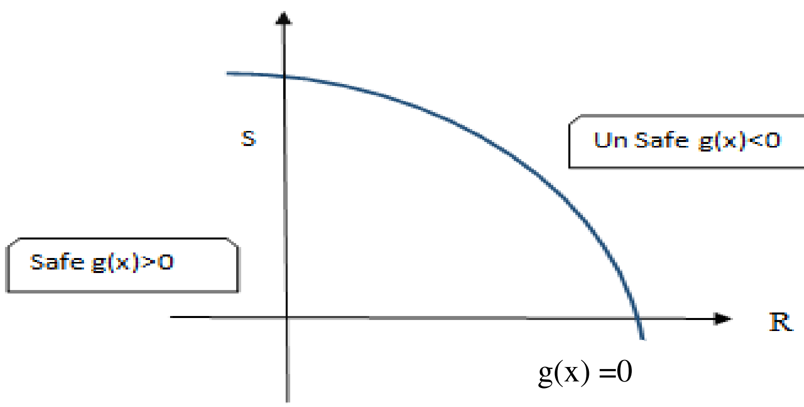

Figure 3.15 The limit state concept

Figure 3.16 Illustrate the corresponding contours and the joint probability density function. The contours are projections of the surface of fx (x_1, x_2) on x_1- x_2 plane. All points on the contours have the same values of f (x) or the same probability density.

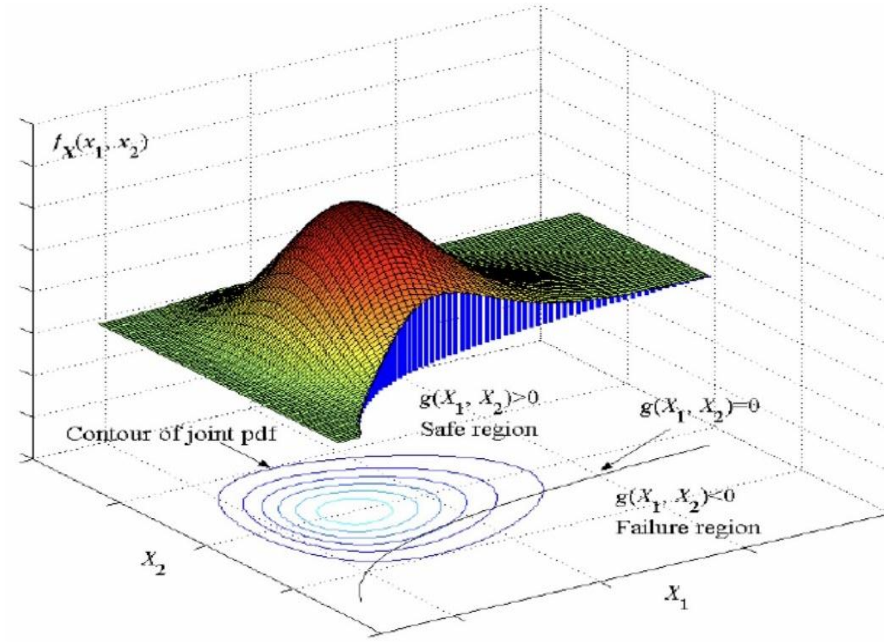

Figure 3.16 Safe and unsafe regions (Manoj, 2016)

3.4.3 First Order Reliability Methods (FORM)

This section introduces some theories behind the FORM. It relates to the underlying mathematical equation and clarifies the advantages of FORM. The form is considered a good alternative for troublesome Monte Carlo analysis. Accuracy is achieved with less computational complexity and mathematical complexity is compensated. FORM was first proposed by Hasofer et al. (1974). It can handle nonlinear performance functions and correlated nonnormal variables. FORM is also called the mean value first order second moment method (MVFOSM). FORM linearizes the performance function using a Taylor series approximation. Therefore, this is a first order approximation. FORM uses only standard deviation and the mean of variables. The performance marginal state function is:

$$z = R - S \tag{3.39}$$

R and S are known as a normal random variable, so Z can also be inferred as a random variable, that is ($\mu R - \mu s, \sqrt{{\sigma_R}^2 + {\sigma_S}^2}$). Then the probability of failure can be defined as

$$p_f = P(Z < 0) \tag{3.40}$$

$$p_f = \emptyset \left[\frac{0 - (\mu_R - \mu_s}{\sqrt{{\sigma_R}^2 + {\sigma_S}^2}} \right] \tag{3.41}$$

$$p_f = 1 - \emptyset\left[\frac{(\mu_R - \mu_s)}{\sqrt{{\sigma_R}^2 + {\sigma_S}^2}}\right] \quad (3.42)$$

ϕ is the standard normal distribution can be taken from z-table

Thus, the probability of failure is a function of the mean value of Z to its standard deviation.

$$\beta = \frac{\mu_z}{\sigma_z} = \frac{(\mu_R - \mu_s)}{\sqrt{{\sigma_R}^2 + {\sigma_S}^2}} \quad (3.43)$$

In this research r and s refer to the resistance obtained from the adopted codes calculation and actual test results that recorded from the experimental work, respectively.

The reliability percentage (P_s) can be calculated based on the corresponding probability of failure P_f that can be introduced in a cumulative distribution function of the standard normal distribution function in the term of the β.

The probability failure can be calculated from the reliability index as follows.

$$p_f = \emptyset(-\beta) = [\,1 - \emptyset(\beta)] \quad (3.44)$$

$$P_s = (1 - P_f) \times 100 \quad (3.45)$$

These variables are limited to positive values. Thus, a log normal distribution is assumed. A generalized formulation of the performance function can be written as:

$$Z = g(X) = (x_1, x_2, x_3 \ldots, x_n) \quad (3.46)$$

$x_1, x_2, x_3 \ldots, x_n$ represents the random variables in the limit state function as mentioned before.

A Taylor series expansion of the limit state function about the mean gives

$$G = g(\mu_x) + \sum_{i=1}^{n} \frac{\partial g}{\partial x_i}(x_i - \mu_{x_i}) + \frac{1}{2}\sum_{i=1}^{n}\sum_{i=1}^{n} \frac{\partial^2 g}{\partial x_i \partial x_j}(x_i - \mu_{x_i})\left(x_j - \mu_{x_j}\right) + \ldots \quad (3.47)$$

The slope is evaluated as an average value. These calculations make FORM less appealing for practical use, but it is far less complicated than it is supposed to be. To alleviate hypothesized mathematical complexity, the new FORM method uses an iterative constrained optimization algorithm that does not require gradient estimation.

Taylor series expansion is truncated for linear terms to obtain a first order approximation. The mean and variance obtained from the truncation expansion:

$$\mu z \approx g\ (\mu x_1, \mu x_2, \mu x_3 \dots, \mu x_n) \qquad (3.48)$$

$$\sigma_z{}^2 \approx \sum_{i=1}^{n}\sum_{i=1}^{n} \frac{\partial g}{\partial x_i}\frac{\partial g}{\partial x_j}\ cov(x_i, x_j) \qquad (3.49)$$

$cov(x_i, x_j)$ is the covariance of x_i andx_j.

This explains the concept behind Mean Value Of First Order Second Moment Method MVFOSM. This is basically a Taylor Series Approximation, rather it is a linearization of the performance function with the mean value of random variables. However, this linearization was later specified as a limitation. After that, a quadratic approximation of the Taylor series approximation is defined and is called SORM - secondary reliability method. The restrictions of MVFOSM are as follows.

The limit of Mean Value Of First Order Second Moment Method MVFOSM

1. Information on the distribution of variables is completely ignored.

2. Truncation error due to linearization at the average point of the nonlinear limit state function.

3. Mechanically equivalent equations were different but the same safety index was not given.

Therefore, the safety index depends on how the limit state equation is formulated. This was commonly referred to as the invariant problem. In order to overcome the problem of invariance, Hasofer and Lind proposed an advanced primary reliability method. This is described in the next section.

CHAPTER 4

RESULTS

4.1 Investigation Of Results

For the purpose of investigation of the results both bending moment capacities are calculated using the two available codes AISC360-10 and EC4-2004, then they are compared with actual test result by using reliability analysis those mentioned in the published literature. Some samples were selected for validation of the results.

4.2 Beam Investigation

4.2.1 Elected Experimental Data

The data are collected from 22 sources found in the literature, which are included 226 CFST rectangular and circular beams were elected with different strength of concrete (ranging between 17 and 154 MPa), steel yield strength (ranging between 86 and 560 MPa), and relative size as listed in Table 4.1, Table 4.2 shows the reliability percentage for all samples and reliability percentage for each article. The specimens' relative size range for B/H was between (0.26-2.00), B/t between (12.50-105.26), H/t between (2.8-205) and for circular D/t between (12.84-120.91). The elected data that imported from the literature review were tested.

Table 4.1 The reliability percentage for quadrilateral CFST beams

Source	No.of Samples	β_{EC4}	Pf	$P_s\%$	β_{AISC}	Pf	$P_s\%$
(Hassanein *et al*, 2017)	6	0.99	0.83	16.90	-1.063	0.144	85.54
(Bambach *et al.*, 2008)	3	-0.14	0.44	55.57	-0.216	0.420	58.00

Table 4.1 The reliability percentage for quadrilateral CFST beams continue

Source	NO.of samples	β_{EC4}	Pf	P_s%	β_{AISC}	Pf	P_s%
(Chen *et al.*, 2017)	20	-0.07	0.47	52.79	-0.348	0.366	63.31
(Arivalagan .S , 2010)	12	-2.35	0.01	99.06	-2.593	0.005	99.49
(Zhan *et al.*, 2016)	8	-3.12	0.00	99.91	-2.013	0.023	97.72
(Wang *et al.*, 2014)	6	2.20	0.97	0.03	2.351	0.980	2.00
(Silva *et al.*, 2016)	2	-2.26	0.01	98.90	0.462	0.677	32.28
(Wang *et al.*, 2014)	4	-0.84	0.20	79.95	-0.884	0.189	81.06
(Lu *et al.*, 2007)	3	-3.87	0.00	99.99	-3.433	0.001	99.97
(Fang *et al*, 2018)	10	0.30	0.62	38.30	0.468	0.677	32.30
(Yu *et al.*, 2018)	18	-0.24	0.41	59.48	-0.588	0.281	71.90
(Wang *et al.*, 2014)	2	-1.13	0.13	87.10	-3.236	0.001	99.93
(Soundararajan, 2017)	15	-2.26	0.01	98.81	-1.354	0.088	91.15
(Han, 2004)	10	-0.56	0.29	71.23	-0.294	0.385	61.41
(Yang *et al.*, 2017)	8	-0.36	0.36	64.06	-1.112	0.135	86.43
(Silva *et al.*, 2016)	8	-0.35	0.37	63.40	-0.353	0.363	63.68
(Wang *et al.*, 2014)	2	-3.71	0.00	99.99	-3.850	0.001	99.99
(Hassanein *et al* 2017)	2	1.02	0.84	16.00	-1.063	0.144	85.6

Table 4.2 The reliability percentage for circular CFST beams

Source	NO.of samples	β_{EC4}	Pf	P_s%	β_{AISC}	Pf	P_s%
(Xu *et al*, 2016)	6	-0.319	0.379	62.10	-0.303	0.382	61.80
(Yu *et al.*, 2018)	20	-1.400	0.080	91.92	-0.836	0.206	79.39
(Chen *et al* 2017)	18	0.022	0.008	99.20	-0.777	0.219	78.01
(Elchalakani *et al* 2001)	12	-0.150	0.440	56.00	-0.327	0.378	62.17
(Hou *et al.*, 2016)	5	-0.650	0.257	74.22	1.366	0.814	18.60
(Chitawadagi and Narasimhan, 2009)	9	-0.451	0.326	67.36	-0.710	0.238	76.11
(Elchalakani *et al* , 2006)	9	0.397	0.651	34.90	0.155	0.559	44.04

The Tables 4.1 and 4.2 show the reliability percentage for CFST beam. The reliability percentage for each article was different for AISC360-10 and for EC4-2004, it ranged between (2.00-99.99)%, the reliability percentage for all articles were 55.57 and 53.94% for the predicted moment resistance based on the EC4-2004 and AISC360-10 for the beam**.**

4.2 Column Investigation

4.2.2 Elected experimental data for quadrilateral sections

The data are collected from 130 sources found in the literature, which are included 1717 CFST rectangular and circular columns were elected with different strength of concrete (ranging between 10 and 115 MPa), steel yield strength (ranging between 227 and 751 MPa), and relative size as listed in Table 4.4, Table 4.5 shows the reliability percentage for all samples and reliability percentage for each article. The elected data that imported from the literature review were tested. The relative size range for B/H between (0.48-4.23), B/t between (7.18-217.83), H/t between (8.23-205) and for circular section D/t was between (9.06-360).

Table 4.3 The reliability percentage for quadrilateral CFST column

Source	NO.of samples	β_{AISC}	Pf	$P_s\%$	β_{EC4}	Pf	$P_s\%$
(Lai *et al*, 2014)	5	-0.610	0.270	72.9	-0.869	0.192	53.7
(Dundu, 2012)	21	-1.124	0.113	88.6	-0.294	0.389	61.4
(Han *et al*, 2003)	30	-1.096	0.137	86.2	-0.424	0.337	66.2
(Guo *et al*, 2012)	9	-0.753	0.226	77.34	-0.312	0.378	62.19
(Guler *et al*, 2013)	13	-0.2112	0.416	58.3	0.945	0.826	17.3
(Mursi and Uy, 2004)	16	-1.0315	0.151	84.8	-0.099	0.464	53.5
(Ishvarbhai *et al*, 2014)	17	-0.2135	0.416	58.3	-0.520	0.301	69.8
(Hao and Lan, 2013)	18	-0.869	0.189	81.06	-0.444	0.330	67.00
(Zhu *et al.*, 2017)	10	-0.816	0.209	79.10	-0.704	0.242	75.80
(Uy *et al* , 2011)	6	-0.523	0.301	69.85	-0.322	0.374	62.55
(Bedage *et al*, 2015)	6	-0.433	0.333	66.65	-0.162	0.436	56.36

Table 4.3 The reliability percentage for quadrilateral CFST column continue

Source	NO.of samples	β_{AISC}	Pf	$P_s\%$	β_{EC4}	Pf	$P_s\%$
(Chu, 2014)	3	-1.485	0.069	93.06	-1.485	0.069	93.02
(Du *et al*, 2016)	8	-0.620	0.267	73.24	-0.469	0.322	67.72
(Liu, 2006)	8	-0.811	0.209	79.10	0.031	0.488	51.20

Table 4.4 The reliability percentage for circular CFST column

Source	NO.of sample	β_{AISC}	Pf	$P_s\%$	β_{EC4}	Pf	$P_s\%$
(Uy *et al*, 2011)	12	-0.387	0.352	64.80	-0.274	0.393	60.64
(Ekmekyapar, 2016)	18	-0.507	0.308	69.15	0.004	0.500	50.00
(Xu *et al*, 2014)	10	-0.046	0.499	50.01	0.342	0.633	36.69
(Lu *et al.*, 2015)	30	-1.240	0.107	89.25	-0.167	0.436	56.36
(Chu, 2014)	6	-1.084	0.140	85.99	1.919	0.971	2.81
(Niranjan and Eramma, 2014)	13	-2.108	0.017	98.21	-1.553	0.060	93.94
(Hamidian *et al.*, 2016)	3	-3.886	0.001	99.99	3.506	0.999	0.20
(Han and Yang, 2005)	8	-1.038	0.151	84.85	-0.373	0.355	64.43

Table 4.4 The reliability percentage for circular CFST column continue

Source	NO.of sample	β_{AISC}	Pf	$P_s\%$	β_{EC4}	Pf	$P_s\%$
(Chen *et al* , 2015)	12	0.423	0.662	33.72	1.613	0.946	5.37
(Abed *et al*, 2013)	6	-0.883	0.189	81.06	-0.881	0.189	81.01
(Sulthana, 2017)	5	1.116	0.866	13.35	2.576	0.854	14.60
(Khan *et al.*, 2017)	16	0.014	0.504	49.60	0.143	0.555	44.43
(Han *et al.*, 2011)	12	-0.759	0.223	77.64	-0.082	0.468	53.19

The tables 4.3 and 4.4 have different reliability percentage for each article it ranged between (0.20-99.99) This difference occurs because of different test results due to different equipment used in the laboratory. The reliability percentage for all articles were 54.95 and 73.32 for the predicted axial load resistance based on the EC4-2004 and AISC360-10 for columns.

4.3 Beam-column investigation for quadrille and circular

4.3.1 Elected Experimental Data for quadrilateral sections

The data are collected from 5 sources for 58 samples found in the literature, were elected with different strength of concrete (ranging between 20 and 290 MPa), steel yield strength (ranging between 253 and 781 MPa), the relative size was B/H between (0.5-2.0), B/t between (7.8-198.3), H/t between (7.8-198.3) and for circular section D/t was between (25-160). Table 4.7show the reliability percentage for each article.

Table 4.5 The reliability percentage for all beam-column members of CFST

Source	NO.of sample	β_{AISC}	Pf	P_s%	β_{EC4}	Pf	P_s%
(Li *et al.*, 2017)	12	-0.694	0.245	75.49	-0.487	0.315	68.44
(Du *et al.*, 2017)	8	0.276	0.606	39.36	0.043	0.516	48.80
(Yu *et al*, 2008)	20	-0.278	0.393	60.64	-0.004	0.500	50.00
(Uy, 2000)	17	-0.038	0.490	51.00	-0.400	0.344	65.54
(Nakahara and Sakino, 1923)	11	-0.343	0.366	63.31	-0.960	0.161	83.89
(Conference and Engineering, 2004)	19	-0.402	0.344	65.54	-2.147	0.015	98.50

Table 4.5 illustrate the reliability percentage for beam-column members the studies of these members CFST was less than from beam and column studies, the reliability percentage ranged between (39.36-98.50) for each article and the reliability percentage for all articles were 69.19 and 59.14 for the predicted moment resistance based on the EC4-2004 and AISC360-10.

4.4 Evaluation of the Codes' Equations

As a first step of the evaluation, the of the effectiveness of the codes prediction of the ultimate moment resistance is by evaluating the effectiveness of the main parameters such as the relative size of the composite materials (concrete and steel). Figure 4.1, 4.2, 4.3, and 4.4 shows the effect of variation of the moment of inertia of the concrete core with respect to the moment of inertia of the surrounding steel on the ultimate moment and load for the rectangular beam, rectangular column, circular beam, and circular column. The comparisons between the two codes (EC4 and AISC) shows that the EC4 is less conservative than the AISC, where the 23% of the elected specimens was overestimated by the code, while 14% of the specimens were overestimated based on the AISC.

Figure 4.5, 4.6, 4.7, and 4.8 shows the effect of the differences in the materials' strength on the normalized moments and loads for the rectangular beam, rectangular column, circular beam, and circular column. In spite of the confinement of the concrete is increasing the compressive strength, but the low differences between the steel and concrete strength show a significant influence on the prediction of the moment resistance for both codes, AISC shows significant scattering for low f_y/f'_c compared to EC4. For L/H, where the increase in L/H decreases the error between the predicted moments, this is clearly can be seen in AISC.

Comparison between the assessment based on the C.O.V and the FORM shows that the linear approximation errors may be magnified by the FORM because it is underestimated the confidence percentages in term of probability of failure, due to considering the contribution of the zone between the design and experimental (Khan, 2016), where the i.e. less than 3% variation. While the differences in C.O.V was 19% for differences between the two codes as mentioned above.

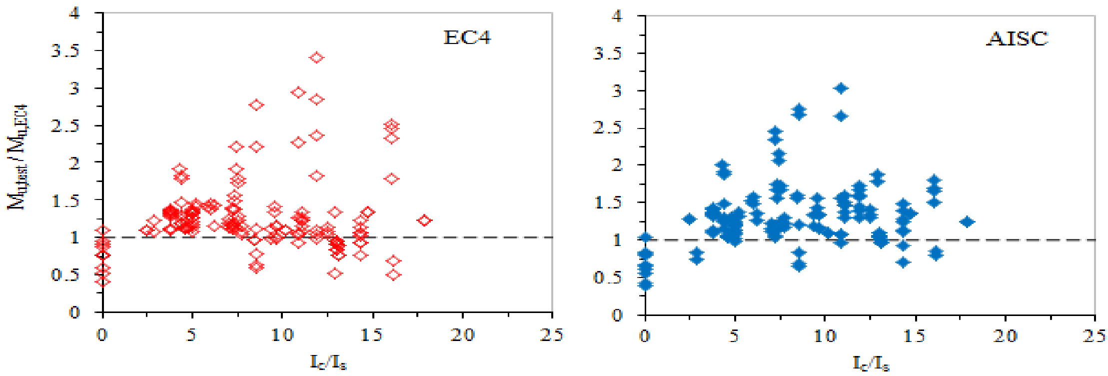

Figure 4.1 Effect of the composite size on the normalized ultimate moment according to EC4 & AISC for a rectangular beam

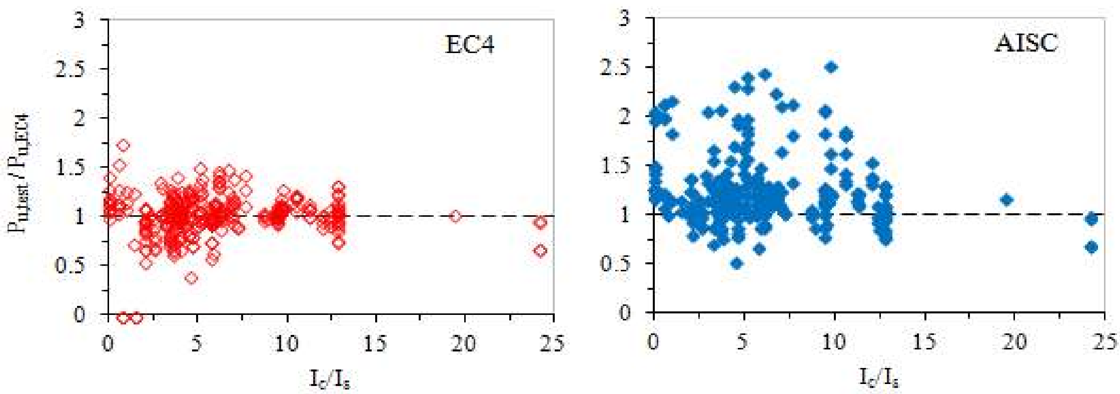

Figure 4.2 Effect of the composite size on the normalized ultimate axial load according to EC4 & AISC for rectangular column

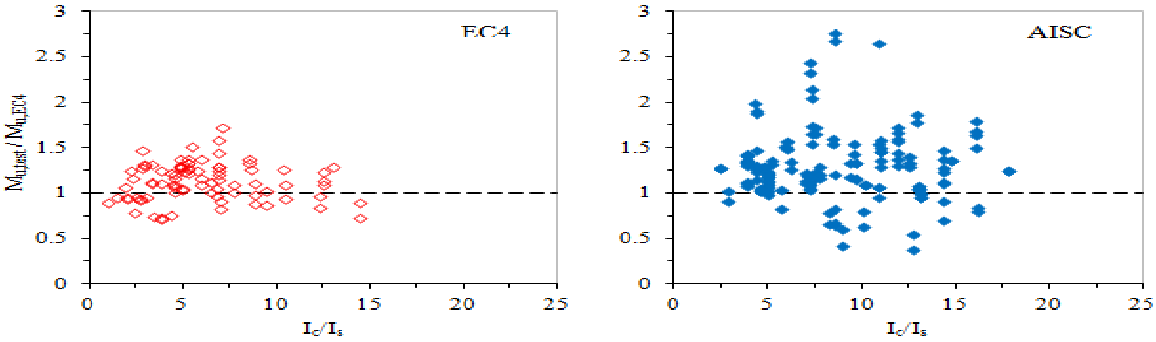

Figure 4.3 Effect of the composite size on the normalized ultimate moment according to EC4 & AISC for a circular beam

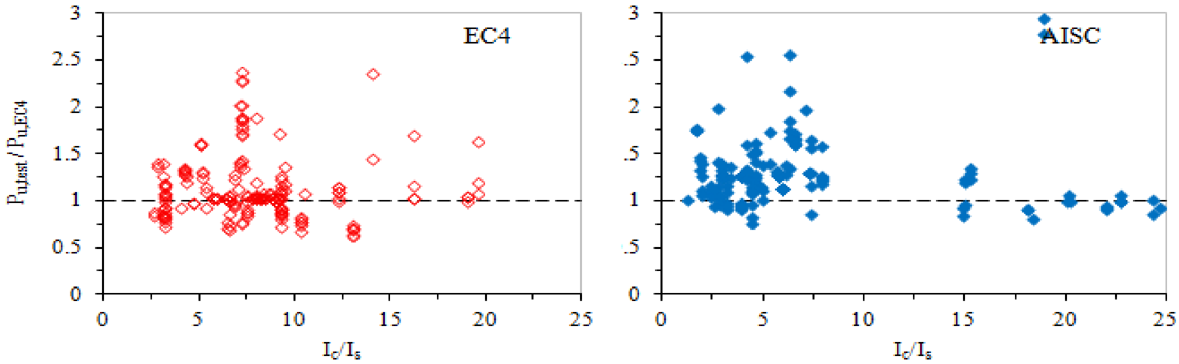

Figure 4.4 Effect of the composite size on the normalized ultimate axial load according to EC4 & AISC for circular column

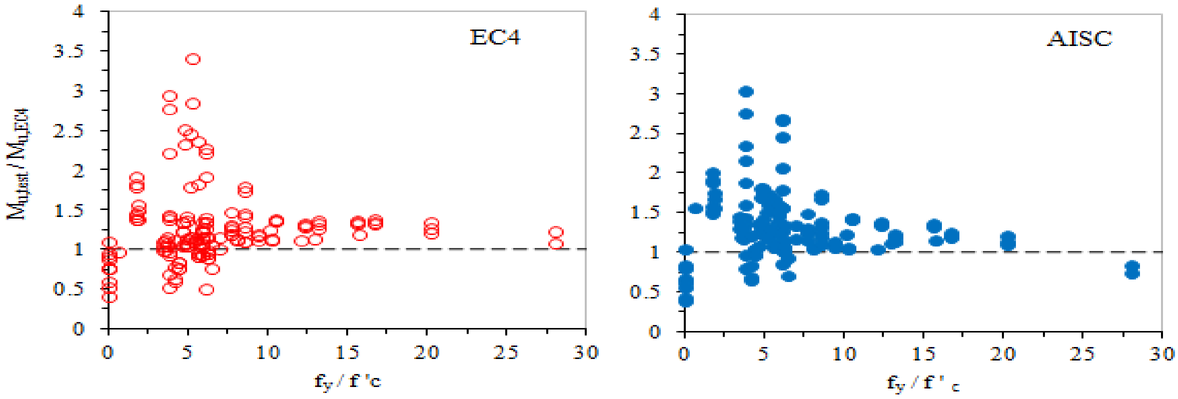

Figure 4.5 Effect of the materials strength percentages on the normalized ultimate moment according to a) EC4 b) AISC for a rectangular beam

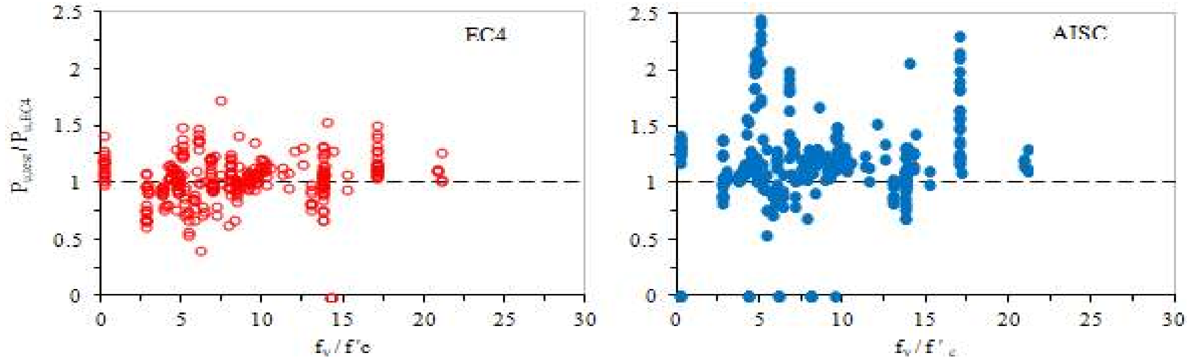

Figure 4.6 Effect of the materials strength percentages on the normalized axial load moment according to a) EC4 b) AISC for rectangular column

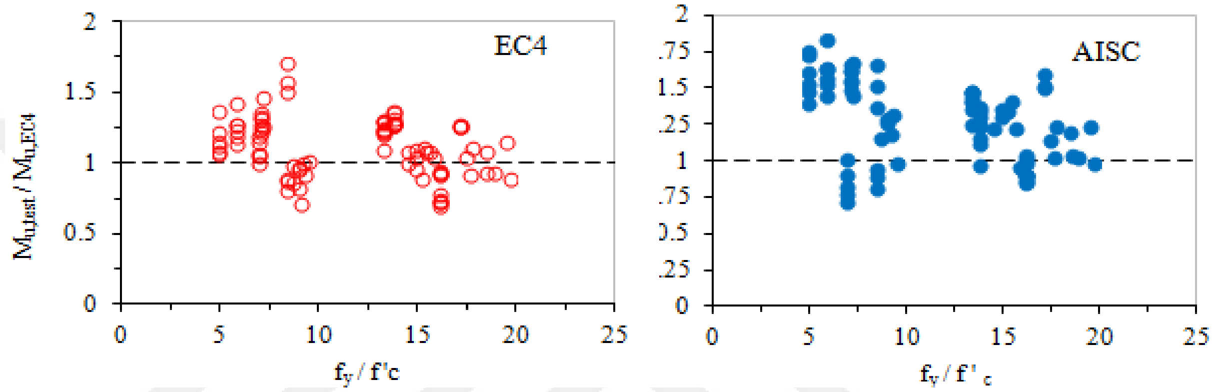

Figure 4.7 Effect of the materials strength percentages on the normalized ultimate moment according to a) EC4 b) AISC for a circular beam

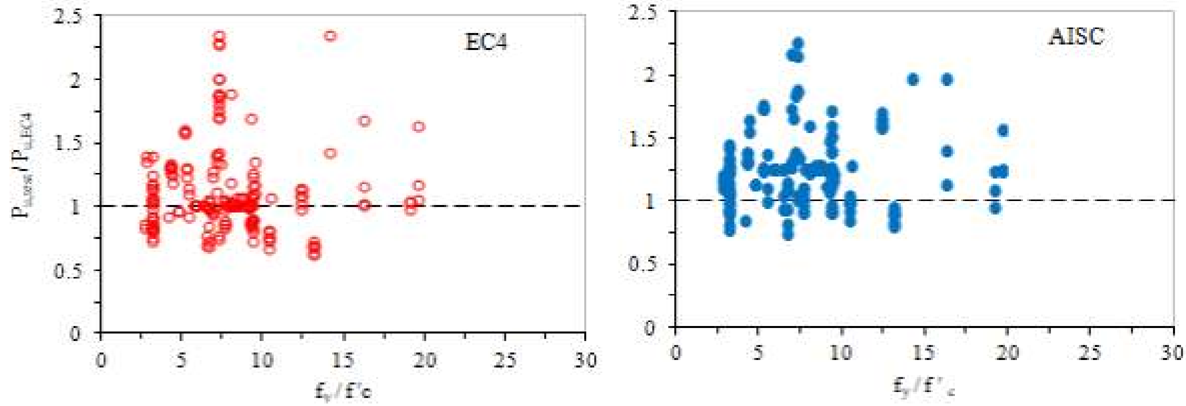

Figure 4.8 Effect of the materials strength percentages on the normalized ultimate moment according to a) EC4 b) AISC for circular column

4.3 The Results and Discussion

There are more than 2500 of different sections were studied. The bending moment capacity and an axial load of these were calculated based on AISC360-10 and EC4-2004 codes.

As a first step of the evaluation, the of the effectiveness of the codes prediction of the ultimate moment resistance and axial load is by evaluating the effectiveness of the main parameters, in order to investigate for which parameters have a greater effect. A reliability method which is a statistical method was used for the purpose of analysis. For all sections used in the study, different parameters including section's (diameter, height, width, thickness, compressive strength of concrete and yield stress of steel) were studied at different values which mainly led to having different ultimate moment resistance and axial load values.

By using reliability analysis, the effect of the tested parameters on both axial load and bending capacity were calculated and the greater impact among those parameters was recorded.

Articles obtained from science direct for the column are more than beam and beam-column while beam-column is the least studied.

The circular and elliptical shape is widely used in the column while in the beam used square and rectangle widely.

CHAPTER 5

CONCLUSION

5.1 Conclusion

In this research, the compressive capacity of the CFST beams, columns, and beam-column under bending moment and axial loads capacities was verified. Two codes were adopted in this study including the AISC360-10 and EC4-2004 are verified to calculate the compressive capacity of CFST beams, columns, and beam-column. The design according to standards is based on finding the capacity subjected to bending moment and axial load capacities. The compression will be made between the actual test result and the theoretical result obtained from AISC360-10 and EC4-2004 codes by reliability analysis. The steps used to design the beam, column, and beam-column using the standards are explained in detail in the separate chapters. The equations to recapitulation the design steps and to make it easier for the reader to understand the equations used. In addition to the design of the CFST beams, columns, and beam-column manually, a spreadsheet solver was developed using Microsoft Excel software for the two standards and reliability index. The spreadsheet solver helps the user to design and check the safety of any section of CFST column and beam, by inserting a few input parameters.

There are several factors that affect to the capacity of the CFST beams, columns, and beam-column. Geometrical and material properties such as cross-sectional shape (t), concrete compressive strength ($f_c{}'$), and steel yield strength ($F_y{}'$). Data collected from the literature are used from since direct.

From the aforementioned calculation and comparison following points can be concluded;

- FORM has underestimated the differences between the predicted methods between the two codes, maybe the second order reliability method is more convenient.
- The reliability in percentages were 55.57 and 53.94% for the predicted moment resistance based on the EC4-2004 and AISC360-10 for beam, for beam-column the reliability percentage were 69.19 and 59.14 for the predicted moment resistance based on the EC4-2004 and AISC360-10 and for the column the reliability percentage is 54.95 and 73.32 for the predicted axial load resistance based on the EC4-2004 and AISC360-10 respectively, while the C.O.Vs the specimens predicted according to EC4 was 0.32 compared to 0.88 according to AISC this is for the beam, for the column the C.O.V 0.22 and 0.49 for EC4 and AISC, and for beam-column C.O.V was 0.25 and 0.5 for EC4-2004 and AISC360-10.
- Comparisons between the two codes provision showed that both codes have percentages of error within the unsafe zone, and EC4 is less conservative than the AISC.
- Increasing the strength of the steel compared to the concrete, are decreases the differences between the predicted in designed specimens for both codes.
- The columns width and height are various contributions of the design codes. These variations are based on the accounting confinement of concrete.
- Comparison between the experimental results and the design codes EC4-2004 and AISC 360-10 results were performed with respect to many factors. Some of them were capable of the cost, section, accuracy of the results and the used equations.

5.2 The Recommendations For Future Studies

The research areas can be expanded, taking in consideration other aspects that are beneficial for achieving the effective design. In order to remedy or solve the problems that may arise when designing all beam, column, and beam-column members other research can address the following points.

1. It recommended studying other methods for reliability analysis such as Monte Carlo Simulation Method or First Order - Second Moment Concept (FOSM).

2. For improvement the bending moment and axial load capacity, it's can be included other standards rather than American and European code such as Japanese code, Chinese code, Canadian code, Australian code etc.
3. It is also proposed to include the study of the effects of shear connectors on the design of beams, columns, and beam-column CFST.
4. Finally, the reinforcement in the design is also recommended.

REFERENCES

Khan, K. N., and Kumar, N. S. (2017) 'Reliability Analysis of Concrete Filled Steel Tubes using ANSYS and First Order Reliability Method', (1979).

Abdalla, S. (2012) 'Behavior of Concrete Filled Steel Tube (CFST) Under Different Loading Conditions', (June), p. 148.

Abed, F., Alhamaydeh, M. and Abdalla, S. (2013) 'Experimental and numerical investigations of the compressive behavior of concrete filled steel tubes (CFSTs)', *Journal of Constructional Steel Research*. Elsevier Ltd, **80**, pp. 429–439. doi: 10.1016/j.jcsr.2012.10.005.

Arivalagan .S, K. (2010) 'Flexural and Cyclic Behavior of Hollow and Concrete-Filled Steel Tubes', *Twentieth International Specialty Conference on Cold-Formed Steel Structures*, pp. 237–254.

Bambach, M. R. *et al.* (2008) 'Hollow and concrete filled steel hollow sections under transverse impact loads', **30**, pp. 2859–2870. doi: 10.1016/j.engstruct.2008.04.003.

Bedage, S D & Shinde, D. N. (2015) 'Concrete Filled Steel Tubes Subjected to Axial Compression', pp. 459–464.

Bucher, C. and Bucher, C. (2011) 'Methods of Reliability Analysis in the context of RDO Methods of Reliability Analysis in the context of RDO'.

Chang, X., Huang, C. K. and Chen, Y. J. (2009) 'Mechanical performance of eccentrically loaded pre-stressing concrete filled circular steel tube columns by means of expansive cement', *Engineering Structures*. Elsevier Ltd, **31(11)**, pp. 2588–2597. doi: 10.1016/j.engstruct.2009.06.007.

Chen, J., Ni, Y. Y. and Jin, W. L. (2015) ‘Column tests of dodecagonal section double skin concrete-filled steel tubes’, *Thin-Walled Structures*. Elsevier, **88**, pp. 28–40. doi: 10.1016/j.tws.2014.11.013.

Chen, Y. *et al.* (2017) ‘Flexural behavior of concrete-filled stainless steel CHS subjected to static loading’, *Journal of Constructional Steel Research*. Elsevier Ltd, **139**, pp. 30–43. doi: 10.1016/j.jcsr.2017.09.009.

Chitawadagi, M. V. and Narasimhan, M. C. (2009) ‘Strength deformation behavior of circular concrete filled steel tubes subjected to pure bending’, *Journal of Constructional Steel Research*. Elsevier Ltd, **65(8–9)**, pp. 1836–1845. doi: 10.1016/j.jcsr.2009.04.006.

Chu, K. (2014) ‘Axial load behavior of steel tube columns in-filled with various high-performance concrete’, pp. 1–114.

The conference, W. and Engineering, E. (2004) ‘13 the World Conference on Earthquake Engineering SEISMIC BEHAVIOR OF STEEL FRAMES WITH OFF-CENTER’, (1787), pp. 1–14.

Ding, F. Xing *et al.* (2018) ‘Behaviour of CFRP-confined concrete-filled circular steel tube stub columns under axial loading’, *Thin-Walled Structures*. Elsevier Ltd, **125**(July 2017), pp. 107–118. doi: 10.1016/j.tws.2018.01.015.

Du, *et al.* (2017) ‘Ultimate resistance behavior of rectangular concrete-filled tubular beam-columns made of high-strength steel’, *Journal of Constructional Steel Research*. Elsevier Ltd, **133**, pp. 418–433. doi: 10.1016/j.jcsr.2017.02.024.

Du, *et al* (2016) ‘Behavior of rectangular concrete-filled high-strength steel tubular columns with different aspect ratio’, *Thin-Walled Structures*. Elsevier, **109**(October), pp. 304–318. doi: 10.1016/j.tws.2016.10.005.

Dundu, M. (2012) ‘Compressive strength of circular concrete filled steel tube columns’, *Thin-Walled Structures*. Elsevier, **56**, pp. 62–70. doi: 10.1016/j.tws.2012.03.008.

Ekmekyapar, T. (2016) ‘Experimental performance of concrete filled welded steel tube columns’, *Journal of Constructional Steel Research*. Elsevier B.V., **117**, pp. 175–184. doi: 10.1016/j.jcsr.2015.10.013.

Elchalakani, M., Zhao, X. and Grzebieta, R. (2006) ‘Variable amplitude cyclic pure bending tests to determine fully ductile section slenderness limits for cold-formed CHS’, **28**, pp. 1223–1235. doi: 10.1016/j.engstruct.2005.10.022.

Elchalakani, M., Zhao, X. L. and Grzebieta, R. H. (2001) ‘Concrete-filled circular steel tubes subjected to pure bending’, *Journal of Constructional Steel Research*, **57(11),** pp. 1141–1168. doi: 10.1016/S0143-974X(01)00035-9.

Elremaily, A. and Azizinamini, A. (2002) ‘Behavior and strength of circular concrete-filled tube columns’, *Journal of Constructional Steel Research*, **58(12)**, pp. 1567–1591. doi: 10.1016/S0143-974X(02)00005-6.

Fang, C.*et al*. (2018) ‘Cold-formed stainless steel RHSs / SHSs under combined compression and cyclic bending A-A B-B C-C’, *Journal of Constructional Steel Research*. Elsevier Ltd, **141**, pp. 9–22. doi: 10.1016/j.jcsr.2017.11.001.

Guler, *et al* (2013) ‘Behaviour of SFRC Filled Steel Tube’, *Advanced Steel Construction*, **9(1)**, pp. 14–25.

Guo, L. H., *et al* (2012) ‘Experimental Study of Concrete-Filled Rectangular HSS Columns Subjected to Biaxial Bending’, *Advances in Structural Engineering*, **15(8)**, pp. 1329–1344. doi: 10.1260/1369-4332.15.8.1329.

Hadi, M. N. S. (2012) ‘High strength thin-walled rectangular concrete- filled tubular slender beam-columns , Part II : Behaviour’.

Hafiz, F. (2016) ‘Analytical and Numerical Study on Behavior of Concrete Filled Steel Tabular Columns Subjected To Axial Compression Loads’, **7(9)**, pp. 1720–1727.

Hamidian, M. R. *et al.* (2016) ‘Pitch spacing effect on the axial compressive behaviour of spirally reinforced concrete-filled steel tube (SRCFT)’, *Thin-Walled Structures*, **100**, pp. 213–223. doi: 10.1016/j.tws.2015.12.011.

Han, L. H. (2004) ‘Flexural behaviour of concrete-filled steel tubes’, *Journal of Constructional Steel Research*, **60(2)**, pp. 313–337. doi: 10.1016/j.jcsr.2003.08.009.

Han, L. H. *et al.* (2011) ‘Tests on curved concrete filled steel tubular members subjected to axial compression’, *Journal of Constructional Steel Research*. Elsevier Ltd, **67(6)**, pp. 965–976. doi: 10.1016/j.jcsr.2011.01.012.

Han, L. H.*et al*. (2003) ‘Concrete-filled thin-walled steel SHS and RHS beam-columns subjected to cyclic loading', *Thin-Walled Structures*, **41(9)**, pp. 801–833. doi: 10.1016/S0263-8231(03)00030-2.

Han, L. and Yang, Y. (2005) 'Cyclic performance of concrete-filled steel CHS columns under flexural loading', **61**, pp. 423–452. doi: 10.1016/j.jcsr.2004.10.004.

Hao, Y. E. and Lan, Y. Q. (2013) 'Research on the Axial Bearing Capacity of Concrete-Filled Rectangular Steel Tube Short Column', *Applied Mechanics and Materials*, 368–370, pp. 1710–1717. doi: 10.4028/www.scientific.net/AMM.368-370.1710.

Hassanein, M. *et al* F., (2017) 'Experimental investigation of cementitious material-filled square thin-walled steel beams', *Thin-Walled Structures*. Elsevier Ltd, **114**(January), pp. 134–143. doi: 10.1016/j.tws.2017.01.031.

Hou, C. C. *et al.* (2016) 'Flexural behavior of circular concrete filled steel tubes (CFST) under sustained load and chloride corrosion', *Thin-Walled Structures*. Elsevier, **107**, pp. 182–196. doi: 10.1016/j.tws.2016.02.020.

Identity, P. *et al.* (2017) 'Chapter 1', pp. 3–21.

Ishvarbhai, V., Quan, Q. and Hadi, M. N. S. (2014) 'Nonlinear analysis of axially loaded circular concrete- fi lled stainless steel tubular short columns', *Jcsr*, **101**, pp. 9–18. doi: 10.1016/j.jcsr.2014.04.036.

Khan, K. N. (2016) 'RELIABILITY STUDY OF CONCRETE FILLED TUBES USING', (1997), pp. 24–27.

Khan, M. *et al.* (2017) 'Behaviour and design of short high-strength steel welded box and concrete-filled tube (CFT) sections', *Engineering Structures*, **147**, pp. 458–472. doi: 10.1016/j.engstruct.2017.06.016.

Lai, Z., *et al*. (2014) 'Noncompact and slender rectangular CFT members : Experimental database , analysis , and design', *JCSR*. Elsevier Ltd, **101**, pp. 455–468. doi: 10.1016/j.jcsr.2014.06.004.

Lazkani, A. (2016) 'Behavior of Expansive Concrete-Filled Steel Tubular (Ecfst) Columns under Axial Loadings', p. 157. Available at: http://scholarworks.uaeu.ac.ae/all_theses.

Lee, M. and Kang, T. H. (2016) 'Flexural strength of circular concrete - filled tubes',

4(4), pp. 297–313.

Li, G. *et al.* (2017) 'Flexural behavior of high strength concrete filled high strength square steel tube', *Journal of Constructional Steel Research*. Elsevier Ltd, **128**, pp. 732–744. doi: 10.1016/j.jcsr.2016.10.007.

Liu, D. (2006) 'Behaviour of eccentrically loaded high-strength rectangular concrete-filled steel tubular columns', *Journal of Constructional Steel Research*, **62(8)**, pp. 839–846. doi: 10.1016/j.jcsr.2005.11.020.

Lu, F. W. *et al.* (2007) 'Flexural behavior of concrete filled non-uni-thickness walled rectangular steel tube', **63**, pp. 1051–1057. doi: 10.1016/j.jcsr.2006.09.006.

Lu, Y. *et al.* (2015) 'Behavior of steel fiber reinforced concrete-filled steel tube columns under axial compression', *Construction and Building Materials*, **95**, pp. 74–85. doi: 10.1016/j.conbuildmat.2015.07.114.

Lu, Y., Li, N. and Li, S. (2014) 'Behavior of FRP-confined concrete-filled steel tube columns', *Polymers*, **6(5)**, pp. 1333–1349. doi: 10.3390/polym6051333.

Manoj, N. R. (2016) 'First - order Reliability Method : Concepts and Application'.

Mursi, M. and Uy, B. (2004) 'Strength of slender concrete filled high strength steel box columns', *Journal of Constructional Steel Research*, **60(12)**, pp. 1825–1848. doi: 10.1016/j.jcsr.2004.05.002.

Nakahara, H. and Sakino, K. (1923) 'FLEXURAL BEHAVIOR OF CONCRETE FILLED SQUARE STEEL TUBULAR BEAM-COLUMNS', pp. 1–8.

Niranjan, B. R., and Eramma, H. (2014) 'Comparison of Experimental values with EC 4, ACI-318, AISC- LRFD of Concrete Filled Steel Fluted Columns for Concentric Load', **2(05)**, pp. 335–344.

Uy, B. (2000) 'STRENGTH OF CONCRETE FILLED S TEEL B OX COLUMNS', (March), pp. 341–352.

de Oliveira, W. L. A. *et al.* (2009) 'Influence of concrete strength and length/diameter on the axial capacity of CFT columns', *Journal of Constructional Steel Research*, **65(12)**, pp. 2103–2110. doi: 10.1016/j.jcsr.2009.07.004.

Perea, T. (2010) 'Analytical and Experimental Study on Slender Concrete-Filled Steel

Tube Columns and Beam-Columns', (December), p. 703.

Naveen Kumar., *et al* (2016) 'RELIABILITY ANALYSIS OF CFT COLUMN BY SIMULATION APPROCH', pp. 2319–2322.

Khan, K. N. and Kumar, N. S. (2017) 'RELIABILITY ANALYSIS OF CONCRETE FILLED STEEL TUBE COLUMNS BY FOSM AND SUBSET SIMULATION TECHNIQUE', **0072**, pp. 385–388.

Sakino, K. *et al.* (2004) 'Behavior of Centrally Loaded Concrete-Filled Steel-Tube Short Columns', *Journal of Structural Engineering*, **130(2)**, pp. 180–188. doi: 10.1061/(ASCE)0733-9445(2004)130:2(180).

Silva, A. *et al.* (2016) 'Seismic performance of composite moment-resisting frames achieved with sustainable CFST members', *Frontiers of Structural and Civil Engineering*, **10(3)**, pp. 312–332. doi: 10.1007/s11709-016-0345-y.

Soundararajan, A. and Shanmugasundaram, K. (2017) 'Flexural behaviour of concrete - filled steel hollow sections beams', **3730**(January). doi: 10.3846/1392-3730.2008.14.5.

Sulthana (2017) 'Axial Compression Behaviour of Long Concrete Filled Double Skinned Steel Tubular Columns', *Structures*. Institution of Structural Engineers, **9**, pp. 157–164. doi: 10.1016/j.istruc.2016.12.002.

Uy, B., *et al* (2011) 'Behaviour of short and slender concrete-filled stainless steel tubular columns', *Journal of Constructional Steel Research*. Elsevier Ltd, **67(3)**, pp. 360–378. doi: 10.1016/j.jcsr.2010.10.004.

Wang, R. *et al.* (2014) 'Flexural performance of rectangular CFST members', *Thin-Walled Structures*. Elsevier, **79**, pp. 154–165. doi: 10.1016/j.tws.2014.02.015.

Wang, W. H. *et al.* (2014) 'Behavior of concrete-filled steel tubular stub columns and beams using dune sand as part of fine aggregate', *Construction and Building Materials*. Elsevier Ltd, **51**, pp. 352–363. doi: 10.1016/j.conbuildmat.2013.10.049.

Wang, Y. *et al.* (2011) 'Time-dependent behaviour of expansive concrete-filled steel tubular columns', *Journal of Constructional Steel Research*. Elsevier Ltd, **67(3)**, pp. 471–483. doi: 10.1016/j.jcsr.2010.09.007.

Xu, F., *et al*W. L. (2014) 'Experimental investigation of thin-walled concrete-filled steel tube columns with reinforced lattice angle', *Thin-Walled Structures*. Elsevier, **84**, pp. 59–67. doi: 10.1016/j.tws.2014.05.015.

Xu, F., Chen, J. and Jin, W. L. (2016) 'Experimental investigation of concrete-filled steel tubular longitudinal gusset plate connections', *Journal of Constructional Steel Research*. Elsevier Ltd, **124**, pp. 163–172. doi: 10.1016/j.jcsr.2016.04.019.

Yang, Z. *et al.* (2017) 'Flexural behavior of high strength concrete filled square steel tube with inner CFRP circular tube', *KSCE Journal of Civil Engineering*, **21(7)**, pp. 2728–2737. doi: 10.1007/s12205-017-0579-9.

Yu, M. *et al.* (2018) 'A uni fi ed formula for calculating bending capacity of solid and hollow concrete- fi lled steel tubes under normal and elevated temperature', *Journal of Constructional Steel Research*. Elsevier Ltd, **141**, pp. 216–225. doi: 10.1016/j.jcsr.2017.11.017.

Yu, *et al* (2008) 'Experimental behaviour of high performance concrete-filled steel tubular columns', *Thin-Walled Structures*, pp. 362–370. doi: 10.1016/j.tws.2007.10.001.

Zhan, Y. *et al.* (2016) 'Behavior of prestressed concrete-filled steel tube (CFST) beam', *Engineering Structures*, **122**, pp. 144–155. doi: 10.1016/j.engstruct.2016.04.050.

Zhu, A. *et al.* (2017) 'Experimental study of concrete filled cold-formed steel tubular stub columns', *Journal of Constructional Steel Research*. Elsevier Ltd, **134**, pp. 17–27. doi: 10.1016/j.jcsr.2017.03.003.